MCP Papers in Press. Published on August 9, 2011 as Manuscript M111.008094

Proteomic profiling of adipose tissue from Zmpste24$^{-/-}$ mice, a model of lipodystrophy and premature aging, reveals major changes in mitochondrial function and vimentin processing

Juan R. Peinado[+¶], Pedro M. Quirós*, Marina R. Pulido[+], Guillermo Mariño*, Maria L. Martínez-Chantar[#], Rafael Vázquez-Martínez[+], José M.P. Freije*, Carlos López-Otín* and María M. Malagón[+¶].

[+]Department of Cell Biology, Physiology and Immunology, University of Córdoba. Instituto Maimónides de Investigación Biomédica de Córdoba (IMIBIC), Córdoba, Spain. CIBER Fisiopatología de la Obesidad y Nutrición (CIBERobn), Instituto de Salud Carlos III, Spain.
*Department of Biochemistry and Molecular Biology, Universidad de Oviedo, Instituto Universitario de Oncología (IUOPA), Oviedo, Spain.
[#]CIC bioGUNE, CIBER de Enfermedades Hepáticas y Digestivas (CIBERehd).

[¶] To whom correspondence should be addressed: Department of Cell Biology, Physiology and Immunology. Campus Universitario de Rabanales. Edificio Severo-Ochoa, Pl. 3. University of Córdoba. E-14014 Córdoba. Spain. Phone: +34 957 21 22 56. Fax: +34 957 21 86 34. E-mail: bc1mapom@uco.es; bc2pemej@uco.es.

Running title: Proteomic profile of lipoatrophy

Abbreviations: BAT, Brown adipose tissue; CPT1, Carnitine palmitoyltransferase I; 2-DE, Two-dimensional gel electrophoresis; DAG, Diacylglycerol; FA, Fatty acid; FPLD, Dunnigan-type familial partial lipodystrophy; HIV, Human immunodeficiency virus; HMGB1, High-Mobility Group Box-1 protein; IPA, Ingenuity Pathway Analysis; LMNA, Lamin A; LPC, Lysophosphatidylcholine; MAG, Monoacylglycerol; MS, Mass spectrometry; SVF, Stromal vascular fraction; TCA, Tricarboxylic acid cycle; TGA, Triacylglycerol; UCP-1, Uncoupling protein 1.

SUMMARY

Lipodystrophy is a major disease involving severe alterations of adipose tissue distribution and metabolism. Mutations in genes encoding the nuclear envelope protein lamin A or its processing enzyme, the metalloproteinase Zmpste24, cause diverse human progeroid syndromes that are commonly characterized by a selective loss of adipose tissue. Similarly to humans, mice deficient in Zmpste24 accumulate prelamin A and display phenotypic features of accelerated aging, including lipodystrophy. Herein, we report the proteome and phosphoproteome of adipose tissue as well as serum metabolome in lipodystrophy by using *Zmpste24*$^{-/-}$ mice as experimental model. We show that Zmpste24 deficiency enhanced lipolysis, fatty acid (FA) biogenesis and β-oxidation as well as decreased FA re-esterification, thus pointing to an increased partitioning of FA toward β-oxidation and away from storage that likely underlies the observed size reduction of *Zmpste24*-null adipocytes. Besides the mitochondrial proteins related to lipid metabolism, other protein networks related to mitochondrial function, including those involved in tricarboxylic acid cycle (TCA) and oxidative phosphorylation, were up-regulated in *Zmpste24*$^{-/-}$ mice. These results, together with the observation of an increased mitochondrial response to oxidative stress, support the relationship between defective prelamin A processing and mitochondrial dysfunction and highlight the relevance of oxidative damage in lipoatrophy and aging. We also show that absence of Zmpste24 profoundly alters the processing of the cytoskeletal protein vimentin and identify a novel protein dysregulated in lipodystrophy, High-Mobility Group Box-1 Protein (HMGB1). Finally, we found several lipid derivates with important roles in energy balance, such as Lysophosphatidylcholine (LPC) or 2-arachidonoylglycerol, to be dysregulated in *Zmpste24*$^{-/-}$ serum. Together, our findings in *Zmpste24*$^{-/-}$ mice may be useful to unveil the mechanisms underlying adipose tissue dysfunction and its overall contribution to body

homeostasis in progeria and other lipodystrophy syndromes as well as to develop novel strategies to prevent or ameliorate these diseases.

INTRODUCTION

Adipose tissue has emerged as one of the most important organs regulating body homeostasis as it serves not only for the storage of energy in the form of triglycerides but it is also a source of paracrine and endocrine signals (i.e. adipokines) that influence systemic metabolism (1-4). Dysfunction of adipose tissue, as occurs in conditions of excess (obesity) or reduced (lipodystrophy) body fat, results in an abnormal management of triglycerides and alteration of adipokine secretion, leading to several metabolic disturbances such as insulin resistance, dyslipidemia, hepatic steatosis and type 2 diabetes (4-5). Accordingly, much effort has been made to elucidate the molecular mechanisms underlying adipose tissue dysfunction and its role in the development of metabolic diseases, including the utilization of proteomic approaches [reviewed in (6-7)]. Indeed, both the number and quality of adipose tissue proteomic studies have notably increased in the last years. Thus, proteome studies have been conducted on adipose tissue biopsies from different fat depots (i.e. visceral and subcutaneous adipose tissue) (8) as well as on the two fractions comprising adipose tissue, mature adipocytes and the stromal vascular fraction (SVF) (9). Isolation of the separate cellular components of the latter fraction has also enabled to establish the proteome of adipose-derived adult stem cells and adipogenesis (10-12). Moreover, novel adipose tissue secreted peptides and proteins have been identified using proteomic techniques (6, 13-14) .

Since obesity is the most prevalent condition affecting adipose tissue function, the vast majority of the proteomic studies carried out to date have focused on the molecular characterization of adipose tissue from obese human (8, 15), mouse (16-17), or rat (18-19) models. Actually, no other pathological states of adipose tissue have been investigated so far using proteomic techniques. In this regard, lipodystrophy, which includes a variety of distinct syndromes that may be inherited or acquired in origin, is characterized by a generalized or

partial lack of adipose tissue [reviewed by (5, 20)]. Inherited lipodystrophies are commonly associated to mutations in single genes whereas acquired lipodystrophies develop in patients with certain autoimmune diseases and, more often, in HIV-infected patients under antiretroviral therapy [reviewed by (5, 21-22)].

The most common genetic disorders of inherited lipodystrophies have been linked to mutations in the *LMNA* gene encoding the nuclear envelope A-type lamins, lamins A and C (5). Although these proteins are expressed in nearly all cell types, mutations in *LMNA* are responsible for at least a dozen different disorders with tissue-selective affections and collectively referred to as laminopathies, including Dunnigan-type familial partial lipodystrophy (FPLD) (23). In addition to a structural role, lamins are also involved in the regulation of DNA replication, transcription and repair (24). In the case of adipose tissue, it has been suggested that lamins play a role in adipocyte differentiation yet the molecular mechanisms responsible for the loss of adipose tissue associated to lamin A/C deficiency are not completely understood [reviewed by (5, 24)]. In humans, mutations in the gene encoding the zinc metalloproteinase Zmpste24/FACE1, which is involved in the post-translational cleavage of carboxy-terminal residues of farnesylated prelamin A to form mature lamin A (25) (Fig. 1), cause progeroid syndromes (i.e. restrictive dermopathy and mandibuloacral dysplasia) characterized by a generalized loss of fat, especially pronounced in extremities and the truncal region (23-24). Similarly to humans, mice lacking Zmpste24 accumulate prelamin A and display phenotypic features of progeria including also a generalized lipodystrophy (26), as well as substantial changes in circulating plasma levels of several adipokines (27), hormones and growth factors (28-29).

In order to investigate the exact impact of the impairment of prelamin A processing on the functioning of adipocytes, we have carried out a proteomic study of adipose tissue from

Zmpste24$^{-/-}$ mice. Our findings indicate that the absence of Zmpste24 enhances mitochondrial function, specially TCA cycle and electron transport chain, to such a level that it causes oxidative damage. Other metabolic disturbances directly affecting lipid management, such as fatty acid (FA) β-oxidation and re-esterification, together with alterations in vimentin processing, likely contribute to the lipoatrophic state associated with lamin A-related diseases. Finally, serum metabolomics revealed for the first time several markers of lipodystrophy, mostly lipid compounds, further supporting the relevance of the dysregulation of lipid metabolism in the premature aging phenotype.

EXPERIMENTAL PROCEDURES

Animals

Mutant mice deficient in Zmpste24 metalloproteinase have been previously described (26). A total of 38 animals have been used for these studies (18 *Zmpste24*$^{-/-}$ and 20 wild-type males). Animal procedures were conducted in accordance with the guidelines of the Committee on Animal Experimentation of the University of Oviedo (Oviedo, Spain).

Histological analysis

For histological analysis, adipose tissue samples from the visceral fat pad obtained from 4 *Zmpste24*$^{-/-}$ and 3 wild-type animals were fixed in 4% paraformaldehyde in PBS and stored in 70% ethanol. Fixed tissues were embedded in paraffin by standard procedures. Blocks were sectioned (5 μm) and tissues stained with hematoxylin and eosin. The number of adipocytes and their mean diameter were determined in 5-μm tissue sections by computer-assisted image analysis. For each sample, different microscopic fields were analyzed, and at least 100 adipocytes were measured.

Protein extraction

For proteomic studies, adipose tissue biopsies from 4 *Zmpste24*$^{-/-}$ and 4 wild-type animals were washed in PBS immediately after removal and directly frozen in liquid nitrogen and stored at -80ºC. Samples were processed following a specific protocol previously optimized by us for adipose tissue (9). Thus, fat samples were thawed by adding 0.4 ml of cold urea/thiourea buffer [7 M urea, 2 M thiourea, 4% CHAPS, 45 mM Tris pH 7.4, 60 mM DTT, and complete protease inhibitors (1 tablet/20 ml, Roche, Barcelona, Spain)] supplemented with 0.1 mM NaCl, mechanically disrupted and briefly sonicated. Then, they were adjusted to 900 µl with lysis buffer (20 mM Tris pH 7.4, 100 mM NaCl, 1% Triton and protease inhibitors; Complete, Roche) and incubated for 15 min at 35°C. After cooling on ice for 10 min, 100 µl of 0.1 M Tris, pH 7, and 50 mM $MgCl_2$ were added to the homogenates, which were then incubated with DNase I (30 U, St. Louis, MO) for 10 min on ice. The homogenate was centrifuged (15 min, 10.000g, 4°C) and the aqueous phase between the upper lipid phase and lower cellular debris phase was collected. Extensive delipidation was accomplished by Tri-n-butylphosphate-acetone-methanol precipitation. Precipitated proteins were resuspended in 75 µl of urea/thiourea buffer. After Bradford assay for protein quantification, samples were diluted to 7 µg/µl with urea/thiourea buffer and frozen at -20ºC.

Isoelectric focusing and 2D-PAGE

350 µg (50 µl) of protein from both wild-type and *Zmpste24*$^{-/-}$ mice, were diluted in 300 µl of Rehydratation Buffer and 0.8% of 3-10NL IPG buffer (GE Healthcare, Barcelona, Spain). Immobilized pH gradient strips (18 cm, pH 3–10 NL) were rehydrated overnight in a Ettan IPGPhor 3 System (GE Healthcare) following a stepwise voltage: 300 V for 3 h, linear gradient to 1,000 V for 4 h, linear gradient to 8,000 V for 2 h, and 8,000 V until total Vh

(40,000) is reached. Strips were equilibrated in SDS Equilibration Buffer [75 mM Tris, pH 8.8, 6 M urea, 30% glycerol, 2% SDS] containing 2% DTT for 15 min, followed by a 15-min wash with equilibration buffer containing 2.5% iodoacetamide. Thereafter, proteins were separated on 12% Tris-glycine gels using an Ettan Dalt Six device (GE Healthcare). These conditions resolved proteins with a MW higher than 20 kDa. After migration, gels were stained with SYPRO Ruby dye and/or 0.1% Coomassie brilliant blue G-250, 10% ammonium sulfate, 2% phosphoric acid and 20% methanol. Both stainings gave similar results.

Staining of phosphoproteins was performed using Pro-Q Diamond stain (Bio-Rad Laboratories, Hercules, CA) according to manufacturer's instructions. 300 µg of adipose tissue extracts were set as the minimum protein amount required for a correct identification of phosphorylated proteins. Images of gels stained with Coomassie, SYPRO Ruby or Pro-Q Diamond were captured with the FX system (Bio-Rad).

MALDI-TOF-MS analysis

Spots were excised automatically in a ProPic station (Genomic Solutions, Huntingdon, UK) and subjected to MS analysis. MALDI-ToF-MS analysis were carried out on a 4800 MALDI-ToF/ToF Analyzer (Applied Biosystems/ MDS SCIEX, Concord, Ontario, Canada). Gel specimens were destained twice (30 min, 37 °C) with 200 mM ammonium bicarbonate/40% acetonitrile. Gel pieces dehydrated for 5 min with pure acetonitrile and dried out over 4 h were automatically digested with trypsin according to standard protocols in a ProGest station (Genomic Solutions). MS and MS/MS analyses of peptides of each sample were analyzed in a 4,700 Proteomics Station (Applied Biosystems) in automatic mode. Samples were deposited onto MPep Chips pre-spotted with alpha-cyano-4-hydroxy-cinnamic acid (Sunyx, Germany) using the thin layer affinity method and analyzed with the following

setting: for the MS data, m/z range 800 to 4,000 with an accelerating voltage of 20 kV and delayed extraction, peak density of maximum 50 peaks per 200 Da, and minimal S/N ratio of 10 and maximum peak at 65. Peak lists for MS/MS data sets were generated using the 4000 Series Explorer (TM) RAC Software, version 3.5.3 (Applied Biosystems/ MDS SCIEX, Concord, Ontario, Canada). For the analysis of vimentin isoforms the m/z range was increased from 400 to 4,000.

Peak lists were submitted to Mascot database in order to identify the proteins (Database, NCBInr 12012010 [10320603 sequences; 3520860234 residues]; taxonomy, Mammalia [757310 sequences]). Analysis was limited to peptides of six or more amino acids and maximum one missed cleavage site. Mass tolerance for precursor ions was set to 100 ppm and mass tolerance for fragment ions to 0.2 Da; oxidation of methionine was searched as variable modification and carbamidomethylation of cysteine was set as fixed modification. MS/MS data were also searched against the ENSEMBL *Mus musculus* database using the open source software X!Tandem (http://www.thegpm.org) with similar settings to those employed for Mascot. Peptide false discovery rates (FDR) were determined by a target decoy approach using a reversed database concatenated to the parent forward database (30). A cutoff expectation value of ≤1.0 [significance threshold; expressed as the negative logarithm of E-value] was chosen for individual MS/MS spectra that resulted in a FDR of ≤1%. Other post-translational modifications (i.e. phosphorylation) were also investigated using Expasy proteomic server (FindMod and Aldente). To determine whether protein carbamylation occurred during the preparation of the samples, representative protein extracts from mouse adipose tissue were analyzed by High-Performance Liquid Chromatography and Tandem Mass spectrometry using LTQ-Orbitrap XL mass spectrometer (Thermo Fisher Scientific

Inc.) equipped with a nanoelectrospray ion source (nESI). No carbamylation was detected under these conditions (data not shown).

Immunoblotting

Frozen fat samples from 4 additional wild-type and *Zmpste24*$^{-/-}$ mice distinct from those employed for 2-DE were disrupted in Triton buffer [20 mM Tris pH 7.4, 150 mM NaCl, 1% Triton and complete protease inhibitor] and incubated in the presence of 30 units of DNase I (Sigma) for 15 min on ice. 30-70 µg of protein were loaded on 10% SDS-PAGE and transferred to nitrocellulose membranes (Biotrace, Pall, Germany). After Ponceau staining to ensure equal sample loading, membranes were blocked for 1 h with 5% dried milk in TTBS (TBS buffer with 0.05% Tween-20). Antibodies against peroxiredoxin 3 (PRDX3), prelamin A, β-actin, carnitine palmitoyltransferase I (CPT1), uncoupling protein 1 (UCP-1) and phosphoenolpyruvate carboxykinase 1 (PCK1) were purchased from Santa-Cruz Biotechnology (Heidelberg, Germany). Anti-vimentin antibody was purchased from Biomedal SL (Sevilla, Spain) and anti-malic enzyme 1 (ME1) antibody was from Proteintech Group, Inc. (Manchester, UK). After overnight incubation at 4 ºC with the corresponding primary antibody, membranes were incubated with the appropriate IgG-HRP-conjugated secondary antibody. Immunoreactive bands were visualized with an enhanced-chemiluminescence reagent (Chemiluminescent HRP substrate, Millipore, MA). Optical densities of the immunoreactive bands were measured using ImageJ 1.40g analysis software.

ROS determination

The intracellular reactive oxygen species (ROS) levels were determined using the 2,7'-dichloroflourescein diacetate (DCF-DA) dye (Sigma). White adipose tissue were extracted

from mice and samples were homogenized using PLB (Promega). The lysates were centrifuged at 12,000 g for 5 min at 4ºC, and supernatants were collected. Protein concentration in the supernatants was evaluated by the bicinchoninic acid technique (BCA protein assay kit, Pierce Biotechnology, Rockford, IL). Supernatants (50 µg) were mixed with 25 µM DCF-DA and then incubated at 37ºC for 30 min in the dark. Fluorescence at 485/535 was measured using a LS55 PerkinElmer LifeScience spectrofluorometer. Adipose tissue samples from at least 4 different animals of each genotype were used for measurement of ROS generation.

Serum metabolomics

Sera from eight *Zmpste24*$^{+/+}$ and *Zmpste24*$^{-/-}$ male mice samples were analyzed. A global metabolite profiling UPLC®-MS methodology was employed, where all endogenous metabolite related features, characterized by mass-to-charge ratio *m/z* and retention time Rt, were included in a subsequent multivariate analysis procedure used to study metabolic differences between the different groups of samples (31). Where possible, Rt-*m/z* features corresponding to putative biomarkers were later identified. Sample preparation, LC-MS system, data processing, multivariate data analysis were performed as described previously (32). The top 50 candidate markers resulting from this procedure were selected and subjected to additional statistical testing [fold changes and Wilcoxon rank sum (Mann Whitney) test *p*-values]. Finally, the following procedures were used in an attempt to identify selected markers: a) Mass spectra recorded in the positive and negative ion modes were analyzed to determine the most likely parent (as opposed to metal adducts or fragments) ion *m/z* value and b) The exact mass information obtained, corrected to within a 5 ppm error, was checked against the ChemSpider[10] online database, using the subdatabases: KEGG, Lipid Maps and

Human Metabolome database. Where possible, hit lists were further reduced by comparison of theoretical / measured isotopic patterns.

Data analysis

2-DE gel analysis was performed by PDQuest software (Bio-Rad), version 8.0. Spot volume values were normalized in each gel by dividing the raw quantity of each spot by the total volume of all the spots included in the same gel. Other normalizations provided by the PDQuest software were also performed with similar results. Data were log transformed to meet the requirements of a normal distribution and analyzed with Student's t-test using the statistics tools included in the PDQuest software. Spots which gave significant results (P<0.05) were verified visually to exclude artifacts. Furthermore, statistically significant spots were re-checked by two-tailed unpaired Student's t-test after reevaluation of density with ImageJ 1.40g software.

Statistical analysis used SSPS statistical software, version 11.0 for WINDOWS (SSPS INC., Chicago, IL). Statistical differences in western blot experiments were assessed by two-tailed unpaired Student's t-test. Differences were considered significant at $P < 0.05$. All data are expressed as mean ± S.E.M. For further evaluation, proteins identified by the proteomic study were analyzed using a pathway analysis software [Ingenuity Pathway Analysis (IPA); Ingenuity Systems, Mountain View, CA] to reveal their potential relationships with other proteins and/or intracellular pathways.

RESULTS

Reduced adipose tissue in *Zmpste24*$^{-/-}$ mice

Zmpste24-null mice display a lipodystrophic phenotype characterized by the absence of subcutaneous adipose tissue (26). Herein, we have observed that they also suffer from a marked reduction of the visceral fat depot (Fig. 2A), which in some cases reached more than a 6-fold decrease when compared to that observed in their wild-type littermates. This remaining fat pad can be easily removed together with the gonads (Fig. 2B). Histological examination of hematoxylin-eosin stained sections revealed that visceral adipose tissue from *Zmpste24*$^{-/-}$ mice is composed of small adipocytes (Fig. 2C), which showed almost half the size of those from wild-type animals. Specifically, minimum diameters of adipocytes from *Zmpste24*-null and wild-type mice were 11±2.9 and 18±1.0 μm, respectively, which likely contributes to the increased number of total adipocytes observed in adipose tissue from *Zmpste24*$^{-/-}$ mice (649.60±83.3 *vs.* 443.4±28.5 cells/mm^2 in *Zmpste24*$^{-/-}$ and wild-type mice, respectively).

Adipose tissue of *Zmpste24*$^{-/-}$ mice exhibits altered metabolic pathways

Our proteomic analysis of visceral adipose tissue allowed for the identification of approximately 1,070 spots in a typical two-dimensional gel. Comparative analysis of the proteome of adipose tissue from *Zmpste24*$^{-/-}$ and wild-type mice (four animals per group) revealed that 37 proteins were significantly up-regulated in mutant mice while 9 proteins were down-regulated (Fig. 3A). A representative spot corresponding to pyruvate dehydrogenase beta (spot 31) is highlighted in Fig. 3B in order to show the reproducibility of the observed differences between adipose tissue proteomes from the two groups of animals. Differences in the proteome of the four different animals analyzed per group were evaluated and average of their density was used to elaborate Table 1, where only those proteins with consistent differences ($P < 0.05$) were included. MALDI-TOF identification of the modified proteins showed that the majority of the spots corresponded to proteins participating in known

metabolic pathways: i) glycolysis (ENO1), ii) Acetyl-CoA synthesis and TCA cycle-related proteins (PC, PDHB, PDX, CS, ACO2, LDH3A, DLST, SUCLG2, SDHA, ME1 and MDH), iii) pentose phosphate pathway (G6PD, PGD, TKT and TALDO1), iv) fatty acid synthesis (FAS and ACLY), v) fatty acid re-esterification (PCK1), vi) β-oxidation of fatty acids (ACSL1 and ACADS), vii) lipolysis [triacylglycerol (TAG) lipase -ATGL- or desnutrin], viii) the glycerol-3-phosphate shuttle (GPD1 and GPD2), and ix) valine, leucine and isoleucine degradation (PCCA, BCATm, HIBADH and HIBCH). Furthermore, several proteins of the mitochondrial electron transport chain (NDUFA10, UQCR1 and ATP5B), the mitochondrial response to oxidative stress (PRDX3), cytoskeleton (vimentin, gelsolin), and proteins with not yet known function in adipose tissue (HMGB1) were also identified. Classical components of the serum were also found to be modified in *Zmpste24*$^{-/-}$ mice (A2M and SERPIN1A).

Herein, we have also observed by 2-DE the accumulation of partially processed lamin A in *Zmpste24*-null mice (Fig 4A). MALDI-TOF/TOF analysis of the protein demonstrated that the accumulated protein lacks the –aaX (Figs. 4B and C) which is consistent with previous findings in *Zmpste24*$^{-/-}$ fibroblasts (33), thus suggesting that, in addition to Zmpste24, other protease(s) (i.e. Rce1) are likely able to carry out this proteolytic step (Fig. 4B). Furthermore, the identified protein contains the sequence including the second proposed cleavage site of Zmpste24 (Figs. 4B and C), indicating that the protein accumulated in mutant animals corresponds exclusively to a partially mature form of lamin A (asterisk in Fig. 4B).

Western blot analysis of altered proteins

Immunoblotting using an antibody against β-actin revealed the existence of significant differences in β-actin protein content between *Zmpste24*$^{-/-}$ and wild-type animals (Supplemental Fig. 1A), thus precluding its use as housekeeping gene for quantitative studies.

Furthermore, neither GADPH nor tubulin gave consistent results (data not shown). Consequently, all the experiments were carried out loading equal amounts of proteins from *Zmpste24*$^{-/-}$ and wild-type mice and values were further normalized against Ponceau staining (Supplemental Fig. 1B).

Several proteins were chosen for validation of the results obtained by 2-DE: three proteins up-regulated (ME1, PRDX3, and HMGB1; Figs. 5A-C) and two down-regulated (PCK1 and vimentin; Fig. 5D and Fig. 6, respectively) in *Zmpste24*$^{-/-}$ mice. These analyses revealed that ME1 was 1.5-fold increased in mutant mice (Fig. 5A) and PRDX3 reached a 4-fold increase (Fig. 5B) in these animals when compared to levels observed in wild-type mice. Likewise, HMGB1 protein content was significantly higher in *Zmpste24*$^{-/-}$ mice (1.8-fold *vs.* wild-type animals; Fig. 5C) whereas PCK1 was diminished in mutant mice (1.9 fold *vs.* wild-type animals; Fig. 5D). Data from immunoblot studies on vimentin are discussed below.

Differential processing of vimentin in adipocytes from *Zmpste24*$^{-/-}$ mice

Immunoblotting of adipose tissue extracts with the anti-vimentin serum confirmed the data obtained by 2-DE on the existence of four distinct immunoreactive bands of 53, 49, 46 and 43 kDa in mice adipose tissue (Fig. 6A). As observed by the proteomic approach, the smaller isoforms of vimentin were down-regulated in adipose tissue from mutant mice, in particular those of 46 and 43 kDa (Fig. 6A). Interestingly, these two short isoforms of vimentin, together with prelamin A, were identified in the 2-DE experiments as the most differentially expressed proteins between *Zmpste24*$^{-/-}$ and wild-type mice (Table 1). Thus, 46-kDa and 43-kDa vimentin forms were reduced by 3.3- and 5.5-fold, respectively, in the proteome of mutant mice with respect to those observed in wild-type animals (Table 1). These

data are largely in accordance with the results obtained by semiquantitative immunoblotting (Fig. 6B).

Although the presence of vimentin isoforms has also been depicted in proteomic studies of human subcutaneous adipose tissue (15), their origin is not known and no information is yet available as to whether they may arise from alternative splicing or post-translational processing. To address this issue, we first analyzed vimentin isoforms by MALDI-TOF/TOF. The identified proteins correspond to N-terminal truncated variants within the region spanning the first 100 amino acid residues of vimentin (Supplemental Fig. 2). Fig. 6C shows the first N-terminal tryptic peptide identified in each isoform, including their predicted molecular weight and isoelectric point. No cleavage was observed at the C-terminal end since the tryptic product was readily detected in the MALDI mass spectrum of all isoforms (Supplemental Fig. 2).

Analysis of mitochondrial function in *Zmpste24*$^{-/-}$ adipose tissue

Given the finding that two proteins potentially involved in mitochondrial fatty acid β-oxidation, long-chain acyl-CoA synthetase-1 (ACSL1) and acyl-coenzymeA dehydrogenase, short chain (ACADS), were up-regulated in adipose tissue of *Zmpste24*$^{-/-}$ mice, we investigated whether mitochondrial fatty acid import could be also affected in these animals by quantifying protein levels of the key enzyme mediating this process, carnitine palmitoyltransferase I (CPT1) (34). Western immunoblotting of adipose tissue protein extracts revealed that *Zmpste24*$^{-/-}$ mice did indeed contain significantly higher levels of CPT1 than wild-type mice (Fig. 7A).

Since proteomic studies revealed that several proteins of the mitochondrial electron transport chain were up-regulated in the adipose tissue of *Zmpste24*-null mice, including a

subunit of the mitochondrial ATP synthase complex, we hypothesized that ATP levels could be altered in *Zmpste24*-null mice. However, ATP content was not significantly modified in mutant mice (data not shown). In order to evaluate whether an increase in thermogenesis, via induction of uncoupling protein 1 [UCP-1; (35-36)], could occur in *Zmpste24*-null mice, we investigated its expression by western blot. No immunoreactive band for UCP-1 was observed in these samples whereas this protein was clearly visible in immunoblots from paired samples of brown adipose tissue (Fig. 7B).

Finally, the increased levels of mitochondrial PRDX3 found in *Zmpste24*$^{-/-}$ fat prompted us to evaluate the occurrence of oxidative damage in the tissue. As shown in Fig. 7C, ROS levels were significantly enhanced in adipose tissue of *Zmpste24*$^{-/-}$ mice as compared to wild-type animals, indicating that Zmpste24 deficiency increases oxidative stress.

Analysis of the phosphoproteome of adipose tissue

Phosphorylation is a ubiquitous and fundamental reversible, regulatory mechanism that enables to modify protein function by altering protein stability, cellular location, substrate affinity, complex formation, or activity (37). Herein, together with the analysis of adipose tissue from *Zmpste24*$^{-/-}$ and wild-type mice by 2D-PAGE, we also employed a phosphoproteomic approach to establish the phosphorylation fingerprint of adipose tissue proteins in the presence or absence of the metalloprotease (Fig 8A). This has enabled us to identify, for the first time, six proteins that are regulated in adipose tissue at the post-translational level: the mitochondrial complex I subunit NDUFA10, the ATP citrate lyase (ACLY), the rate-limiting enzyme for triglyceride catabolism in mice, desnutrin (human ATGL1), phosphoglucomutase 1 (PGM-1), desmin, and pyruvate dehydrogenase alpha 1

(PDHA1). In addition, the potential phosphorylation sites of three of these proteins were also identified (Fig. 8B), including three sites already described in PGM-1 (S95, T96 and T115), one in desmin (T42), and a novel phosphothreonine residue in desnutrin (T452), which is close to the two C-terminal serine residues previously reported to be phosphorylated in this protein (38). Finally, three out of the six proteins found to be highly phosphorylated in mouse adipose tissue were also identified by 2D-PAGE on the basis of their overexpression in mutant animals: NDUFA10, ACLY, and desnutrin (Table 1).

Serum metabolic profile of *Zmpste24*$^{-/-}$ mice

Although microscopy and proteomic analysis of adipose tissue of *Zmpste24*-null mice, together with previous data on the occurrence of hepatic steatosis in these animals (27), pointed to the inability of adipocytes to properly store lipids, we observed no changes in serum FA levels in mutant mice (data not shown). To get further clues about the metabolic biomarkers associated to genetic lipodystrophy, we employed a metabolomic strategy. Serum metabolic profiling revealed 32 metabolites up-regulated in *Zmpste24*$^{-/-}$ mice while 22 were found to be down-regulated. 67 % of the identified metabolites corresponded to known compounds (Suppl. Table 1). Analysis of the altered metabolites by a software for pathway analysis revealed major perturbations in lipid metabolism and oxidative scavenging (Fig. 9). Remarkably, most of the down-regulated metabolites corresponded to lysophospholipids and, in particular to several molecular species of lysophosphatidylcholine (LPC). Increased levels of several steroids including corticosterone (1.9 fold change) and aldosterone (4.4 to 12.9 fold change) were also observed in *Zmpste24*$^{-/-}$ mice, suggestive of alterations in adrenal gland function in these animals. Finally, in agreement with previous observations (27), lower levels of glucose were found in mutant mice as compared to wild-type animals.

DISCUSSION

Lipodystrophy is a major disease involving severe alterations of adipose tissue distribution and metabolism. Mutations in genes encoding the nuclear protein lamin A or its processing enzyme, the metalloproteinase Zmpste24, cause diverse human progeroid syndromes and are associated with the development of lipodystrophy. By using mice deficient in Zmpste24, we report for the first time the protein fingerprint of lipoatrophy. We demonstrate that adipose tissue of *Zmpste24*$^{-/-}$ mice exhibit marked alterations in key proteins involved in lipid management and energy expenditure. This, together with an abnormal processing of the cytoskeletal protein vimentin in *Zmpste24*$^{-/-}$ adipocytes, may underlie the lipodystrophic phenotype associated with the loss of functional Zmpste24.

Microscopic data revealed that *Zmpste24*$^{-/-}$ mice contained significantly smaller adipocytes than wild-type mice, thus indicating an impaired fat storage capacity in these cells. Several processes may contribute to decreased TAG accumulation: increased TAG lipolysis, decreased FA uptake or synthesis, decreased FA re-esterification and increased FA release or oxidation. Our proteomic data support the view that several of these processes may occur in *Zmpste24*-null adipocytes (Fig. 10). Thus, the observed up-regulation of the rate-limiting lipolytic enzyme adipose triglyceride lipase (human ATGL/murine desnutrin) (39) in mutant mice strongly suggest that TAG lipolysis is enhanced in these animals. Intriguingly, we have identified a novel phosphorylation site in desnutrin (T452), which is close to the two C-terminal region serines previously reported to be phosphorylated in this protein (S406 and S430) (38). It has been recently shown that phosphorylation at S406 or S430 is not necessary for the hydrolase activity of desnutrin although the C-terminal region appears to be important

for TAG hydrolysis (40). Thus, it seems likely that phosphorylation at T452 plays a role in the regulation of desnutrin activity.

One of the most increased proteins in adipose tissue of null mice was fatty acid synthase (FAS), an enzyme that plays a central role in *de novo* FA biogenesis. FAS converts acetyl-CoA and malonyl-CoA into palmitate in a process that requires NADPH, which is supplied by both the pentose phosphate pathway and the pyruvate cycle (41). Interestingly, many of the enzymes participating in these pathways were also enhanced in adipose tissue of *Zmpste24*$^{-/-}$ mice. Taken together, these findings suggest that *de novo* lipogenesis is increased in mutant mice. In this scenario, the bulk of FA synthesized *de novo* or generated by TAG hydrolysis does not seem to be redirected for esterification into TAG in *Zmpste24*-null adipocytes since, besides the aforementioned reduced size of these cells, adipose tissue from mutant mice exhibited diminished levels of the key enzyme involved in glyceroneogenesis and FA re-esterification in adipocytes, PCK1 (42). In line with these findings, targeted ablation of PCK1 expression in white adipose tissue in mice reduced body fat pads and, more notably, nearly 25% of the mutant mice were lipodystrophic (43). Likewise, ritonavir, a common component of the antiretroviral therapy associated with the development of lipodystrophy in HIV patients (38), decreased PCK1 expression in murine 3T3-L1 adipocytes (44). Collectively, these observations favour PCK1 as a common player in the development of lipodystrophy.

Impaired FA re-esterification resulting from down-regulation of PCK1 could lead to enhanced FA efflux from *Zmpste24*-null adipocytes and subsequent ectopic deposition of lipids. Indeed, *Zmpste24*-null mice display a clear hepatic steatosis (27). Nevertheless, we (data not shown) and others (27) have found that serum FA levels are not elevated in *Zmpste24*-null mice and thus, it is unlikely that FA from adipose tissue contribute to the

extensive lipid accumulation observed in mutant mice liver (27). Instead, lack of Zmpste24 seems to cause a shift within adipocytes towards increased FA utilization and energy expenditure. Thus, mutant mice exhibited enhanced levels of two enzymes involved in FA β-oxidation (ACSL1 and ACADS). These data, which are consistent with the observed upregulation of CPT1, the enzyme responsible of FA translocation across the mitochondrial membrane (45), support the view that adipocyte shrinkage in mutant mice is due, at least in part, to an increased partitioning of FA toward β-oxidation and away from storage as TAG. Furthermore, the increased expression of several proteins associated with oxidative phosphorylation suggests that adipose tissue metabolism in mutant mice could be remodelled toward ATP production, which is rapidly mobilised to sustain the enhanced rate of FA synthesis. Notably, expression of UCP-1, normally found only in brown adipose tissue but that can be induced in white adipocytes by different stimuli (35-36) was not altered in *Zmpste24*$^{-/-}$ mice thus suggesting that excess energy is not likely dissipated as heat, at least via UCP-1.

Taken together, our results reveal that the lack of Zmpste24 alters mitochondrial function and oxidative capacity of adipocytes. Indeed, a total of 21 out of the 37 proteins overexpressed in *Zmpste24*$^{-/-}$ mice corresponded to mitochondrial proteins involved in oxidative metabolism. Considering the prominent role of adipose tissue mitochondria in lipogenesis and adipogenesis (46), it is reasonable to propose that mitochondrial alterations caused by Zmpste24 depletion contribute to the lipoatrophic phenotype of mutant mice. Remarkably, antiretroviral treatment of HIV patients which causes severe lipoatrophies, altered the expression of genes involved in FA oxidation, TCA cycle and oxidative phosphorylation in adipose tissue (47-49). These changes were associated to up-regulation of genes involved in oxidative stress (49-50). In particular, HIV antiretroviral protease inhibitors

(PIs), which inhibit Zmpste24 activity and lead to prelamin A accumulation (51), induce the expression of oxidative stress markers in adipose tissue in a manner comparable to that observed in patients with *LMNA* mutations (52). In accordance with these observations, evidence supporting the occurrence of oxidative stress in adipose tissue of *Zmpste24*$^{-/-}$ mice is provided by our findings of increased ROS levels. Taking into account that PRDX3 provides a primary antioxidant defense of mitochondrial respiratory chain (53-54), increased ROS levels may account for the significant up-regulation of this peroxidase. Taken together, these findings evidence the relationship between defective prelamin A processing and oxidative stress and highlight the relevance of oxidative damage in the development of lipoatrophy. Interestingly, mitochondrial dysfunction and oxidative stress induced by antiretroviral drugs or prelamin A accumulation have been proposed to promote premature cellular senescence of preadipocytes (52). Our data on *Zmpste24*$^{-/-}$ mice, which exhibit clear features of accelerated senescence, reinforce the notion of a functional link between defective lamin A maturation, mitochondrial alterations and premature aging (55). Notably, Zmpste24 also altered normal processing of the cytoskeletal protein vimentin, an intermediate filament that has been suggested to regulate mitochondrial function by mediating the interaction of mitochondria with microtubules (56). In addition, vimentin has a prominent role in the development of lipid droplets during adipocyte differentiation (57-58) and in the control of lipid metabolism in differentiated adipocytes (59) and, consequently, the presence of vimentin variants may be necessary to provide plasticity to the adipocyte for correct lipid management.

Our proteomic analysis has enabled the identification of a novel protein dysregulated in *Zmpste24*$^{-/-}$ mice, HMGB1, whose expression in adipose tissue has not been documented previously. HMGB1 is a chromatin-binding nuclear protein implicated in DNA repair mechanisms (60), and has been also proposed to play a role in sustaining autophagy (61).

Notably, previous studies have demonstrated that *Zmpste24*$^{-/-}$ mice exhibit an extensive basal activation of autophagy, which primarily represents a pro-survival mechanism, in liver, skeletal muscle and heart (27, 62). In fact, despite the progeroid phenotype of *Zmpste24*$^{-/-}$ mice, these animals also display transcriptional alterations in metabolism regulatory genes in the liver and profound changes in circulating glucose and hormone levels indicative of an activated anti-aging response (27-29). In line with these findings, the shift in the expression profile of metabolic proteins found in *Zmpste24*$^{-/-}$ mice highly resembles that observed in adipose tissue from old rats subjected to calorie restriction (18). Collectively, our proteomic data support the original proposal by Mariño et al. (27) that a protective metabolic response is triggered in *Zmpste24*$^{-/-}$ mice in order to attenuate the deleterious consequences associated to partially processed lamin A accumulation. Despite this adaptive response, continuous mitochondrial overload and subsequent oxidative stress and, presumably, increased autophagy, would finally lead to the loss of adipose tissue observed in mutant mice.

Metabolomic analysis revealed significant changes in plasma metabolites in *Zmpste24*$^{-/-}$ mice. These include the adrenal steroids corticosterone and aldosterone, which were up-regulated in mutant animals. Interestingly, A-ZIP/F-1 mice, a mouse model of lipodystrophy, display high corticosterone serum levels, which can be partially reverted upon leptin treatment (63). Taking into account that circulating leptin is strongly diminished in *Zmpste24*$^{-/-}$ mice (27), its deficiency may contribute, at least in part, to reduce the inhibitory tone on corticosterone secretion by the adrenal gland in these animals. Circulating levels of the endocannabinoid 2-arachidonoylglycerol were highly enhanced in *Zmpste24*$^{-/-}$ animals. There are evidences that endocannabinoids, which control food intake and energy expenditure *via* central actions and are also produced by fat cells and regulate adipose tissue metabolism, are increased in plasma and adipose tissue of obese rodents and human (64). Our present findings

support the view that, as in conditions of excess of body fat, the endogenous endocannabinoid system is also dysregulated in conditions of adipose tissue deficiency. Finally, mutant mice also exhibited a strong down-regulation of different species of the phosphatidylcholine derivate LPC, and both anti-inflammatory (65-66) and pro-inflammatory (67) properties have been attributed for LPCs. Irrespectively of their function, LPCs are increased in obese rats (68) and human (69). Considering the observed LPC depletion in lipoatrophic mice, LPC may therefore constitute a new marker of adipose tissue dysfunction.

In summary, proteomic analysis of adipose tissue from *Zmpste24*$^{-/-}$ mice and measurement of several metabolites in both adipose tissue and serum has enabled us to identify the changes in the protein expression profile and metabolic state associated with lipodystrophy. Our results shed new light on the importance of mitochondrial function for the development of lipodystrophy and for the aging process and link the accumulation of a partially mature form of lamin A to the dysregulation of lipid metabolism and oxidative stress in adipocytes. This, together with our novel findings on the regulation of HMGB1 expression and vimentin processing by Zmpste24, may be useful to unveil the mechanisms underlying adipose tissue dysfunction in laminopathies and other lipodystrophic syndromes as well as to develop novel strategies that may help to prevent or ameliorate these diseases.

REFERENCES

1. Kershaw, E. E., and Flier, J. S. (2004) Adipose tissue as an endocrine organ. *J Clin Endocrinol Metab* 89, 2548-2556.
2. de Luca, C., and Olefsky, J. M. (2006) Stressed out about obesity and insulin resistance. *Nat Med* 12, 41-42; discussion 42.
3. Waki, H., and Tontonoz, P. (2007) Endocrine functions of adipose tissue. *Annu Rev Pathol* 2, 31-56.
4. Fruhbeck, G. (2008) Overview of adipose tissue and its role in obesity and metabolic disorders. *Methods Mol Biol* 456, 1-22.
5. Huang-Doran, I., Sleigh, A., Rochford, J., O'Rahilly, S., and Savage, D. (2010) Lipodystrophy: Metabolic insights from a rare disorder. *J Endocrinol*.
6. Chen, X., and Hess, S. (2008) Adipose proteome analysis: focus on mediators of insulin resistance. *Expert Rev Proteomics* 5, 827-839.
7. Peral, B., Camafeita, E., Fernandez-Real, J. M., and Lopez, J. A. (2009) Tackling the human adipose tissue proteome to gain insight into obesity and related pathologies. *Expert Rev Proteomics* 6, 353-361.
8. Perez-Perez, R., Ortega-Delgado, F. J., Garcia-Santos, E., Lopez, J. A., Camafeita, E., Ricart, W., Fernandez-Real, J. M., and Peral, B. (2009) Differential proteomics of omental and subcutaneous adipose tissue reflects their unalike biochemical and metabolic properties. *J Proteome Res* 8, 1682-1693.
9. Peinado, J. R., Jimenez-Gomez, Y., Pulido, M. R., Ortega-Bellido, M., Diaz-Lopez, C., Padillo, F. J., Lopez-Miranda, J., Vazquez-Martinez, R., and Malagon, M. M. (2010) The stromal-vascular fraction of adipose tissue contributes to major differences between subcutaneous and visceral fat depots. *Proteomics* 10, 3356-3366.
10. DeLany, J. P., Floyd, Z. E., Zvonic, S., Smith, A., Gravois, A., Reiners, E., Wu, X., Kilroy, G., Lefevre, M., and Gimble, J. M. (2005) Proteomic analysis of primary cultures of human adipose-derived stem cells: modulation by Adipogenesis. *Mol Cell Proteomics* 4, 731-740.
11. Roche, S., Delorme, B., Oostendorp, R. A., Barbet, R., Caton, D., Noel, D., Boumediene, K., Papadaki, H. A., Cousin, B., Crozet, C., Milhavet, O., Casteilla, L., Hatzfeld, J., Jorgensen, C., Charbord, P., and Lehmann, S. (2009) Comparative proteomic analysis of human mesenchymal and embryonic stem cells: towards the definition of a mesenchymal stem cell proteomic signature. *Proteomics* 9, 223-232.
12. Kheterpal, I., Ku, G., Coleman, L., Yu, G., Ptitsyn, A. A., Floyd, Z. E., and Gimble, J. M. (2011) Proteome of human subcutaneous adipose tissue stromal vascular fraction cells versus mature adipocytes based on DIGE. *J Proteome Res* 10, 1519-1527.
13. Zhong, J., Krawczyk, S. A., Chaerkady, R., Huang, H., Goel, R., Bader, J. S., Wong, G. W., Corkey, B. E., and Pandey, A. (2010) Temporal profiling of the secretome during adipogenesis in humans. *J Proteome Res* 9, 5228-5238.
14. Roca-Rivada, A., Alonso, J., Al-Massadi, O., Castelao, C., Peinado, J. R., Seoane, L. M., Casanueva, F. F., and Pardo, M. (2011) Secretome analysis of rat adipose tissues shows location-specific roles for each depot type. *J Proteomics*. 74:1068-79.
15. Boden, G., Duan, X., Homko, C., Molina, E. J., Song, W., Perez, O., Cheung, P., and Merali, S. (2008) Increase in endoplasmic reticulum stress-related proteins and genes in adipose tissue of obese, insulin-resistant individuals. *Diabetes* 57, 2438-2444.

16. Jiang, L., Wang, Q., Yu, Y., Zhao, F., Huang, P., Zeng, R., Qi, R. Z., Li, W., and Liu, Y. (2009) Leptin contributes to the adaptive responses of mice to high-fat diet intake through suppressing the lipogenic pathway. *PLoS One* 4, e6884.
17. de Roos, B., Rungapamestry, V., Ross, K., Rucklidge, G., Reid, M., Duncan, G., Horgan, G., Toomey, S., Browne, J., Loscher, C. E., Mills, K. H., and Roche, H. M. (2009) Attenuation of inflammation and cellular stress-related pathways maintains insulin sensitivity in obese type I interleukin-1 receptor knockout mice on a high-fat diet. *Proteomics* 9, 3244-3256.
18. Valle, A., Sastre-Serra, J., Roca, P., and Oliver, J. (2010) Modulation of white adipose tissue proteome by aging and calorie restriction. *Aging Cell* 9, 882-894.
19. Joo, J. I., Kim, D. H., Choi, J. W., and Yun, J. W. (2010) Proteomic analysis for antiobesity potential of capsaicin on white adipose tissue in rats fed with a high fat diet. *J Proteome Res* 9, 2977-2987.
20. Jeninga, E. H., and Kalkhoven, E. (2010) Central players in inherited lipodystrophies. *Trends Endocrinol Metab* 21, 581-588.
21. Garg, A. (2004) Acquired and inherited lipodystrophies. *N Engl J Med* 350, 1220-1234.
22. Villarroya, F., and Domingo, P. (2010) Targets of Metabolic Toxicity of HIV Antiretroviral Drugs: The Multiple Roads to Lipodystrophy and Metabolic Syndrome. *Curr Pharm Des*. 16:3337-8.
23. Worman, H. J., Fong, L. G., Muchir, A., and Young, S. G. (2009) Laminopathies and the long strange trip from basic cell biology to therapy. *J Clin Invest* 119, 1825-1836.
24. Dechat, T., Pfleghaar, K., Sengupta, K., Shimi, T., Shumaker, D. K., Solimando, L., and Goldman, R. D. (2008) Nuclear lamins: major factors in the structural organization and function of the nucleus and chromatin. *Genes Dev* 22, 832-853.
25. Barrowman, J., and Michaelis, S. (2009) ZMPSTE24, an integral membrane zinc metalloprotease with a connection to progeroid disorders. *Biol Chem* 390, 761-773.
26. Pendas, A. M., Zhou, Z., Cadinanos, J., Freije, J. M., Wang, J., Hultenby, K., Astudillo, A., Wernerson, A., Rodriguez, F., Tryggvason, K., and Lopez-Otin, C. (2002) Defective prelamin A processing and muscular and adipocyte alterations in Zmpste24 metalloproteinase-deficient mice. *Nat Genet* 31, 94-99.
27. Marino, G., Ugalde, A. P., Salvador-Montoliu, N., Varela, I., Quiros, P. M., Cadinanos, J., van der Pluijm, I., Freije, J. M., and Lopez-Otin, C. (2008) Premature aging in mice activates a systemic metabolic response involving autophagy induction. *Hum Mol Genet* 17, 2196-2211.
28. Marino, G., Ugalde, A. P., Fernandez, A. F., Osorio, F. G., Fueyo, A., Freije, J. M., and Lopez-Otin, C. (2010) Insulin-like growth factor 1 treatment extends longevity in a mouse model of human premature aging by restoring somatotroph axis function. *Proc Natl Acad Sci U S A* 107, 16268-16273.
29. Ugalde, A. P., Marino, G., and Lopez-Otin, C. (2010) Rejuvenating somatotropic signaling: a therapeutical opportunity for premature aging? *Aging (Albany NY)* 2:1017-22.
30. Elias, J. E., and Gygi, S. P. (2007) Target-decoy search strategy for increased confidence in large-scale protein identifications by mass spectrometry. *Nat Methods* 4, 207-214.
31. Theodoridis, G., Gika, H. G., and Wilson, I. D. (2008) LC-MS-based methodology for global metabolite profiling in metabonomics/metabolomics. *TrAC Trends in Analytical Chemistry* 27, 251-260.

32. Barr, J., Vazquez-Chantada, M., Alonso, C., Perez-Cormenzana, M., Mayo, R., Galan, A., Caballeria, J., Martin-Duce, A., Tran, A., Wagner, C., Luka, Z., Lu, S. C., Castro, A., Le Marchand-Brustel, Y., Martinez-Chantar, M. L., Veyrie, N., Clement, K., Tordjman, J., Gual, P., and Mato, J. M. (2010) Liquid chromatography-mass spectrometry-based parallel metabolic profiling of human and mouse model serum reveals putative biomarkers associated with the progression of nonalcoholic fatty liver disease. *J Proteome Res* 9, 4501-4512.
33. Varela, I., Pereira, S., Ugalde, A. P., Navarro, C. L., Suarez, M. F., Cau, P., Cadinanos, J., Osorio, F. G., Foray, N., Cobo, J., de Carlos, F., Levy, N., Freije, J. M., and Lopez-Otin, C. (2008) Combined treatment with statins and aminobisphosphonates extends longevity in a mouse model of human premature aging. *Nat Med* 14, 767-772.
34. Rufer, A. C., Thoma, R., and Hennig, M. (2009) Structural insight into function and regulation of carnitine palmitoyltransferase. *Cell Mol Life Sci* 66, 2489-2501.
35. Orci, L., Cook, W. S., Ravazzola, M., Wang, M. Y., Park, B. H., Montesano, R., and Unger, R. H. (2004) Rapid transformation of white adipocytes into fat-oxidizing machines. *Proc Natl Acad Sci U S A* 101, 2058-2063.
36. Bogacka, I., Ukropcova, B., McNeil, M., Gimble, J. M., and Smith, S. R. (2005) Structural and functional consequences of mitochondrial biogenesis in human adipocytes in vitro. *J Clin Endocrinol Metab* 90, 6650-6656.
37. Ozlu, N., Akten, B., Timm, W., Haseley, N., Steen, H., and Steen, J. A. (2010) Phosphoproteomics. *Wiley Interdiscip Rev Syst Biol Med* 2, 255-276.
38. Kim, S. C., Chen, Y., Mirza, S., Xu, Y., Lee, J., Liu, P., and Zhao, Y. (2006) A clean, more efficient method for in-solution digestion of protein mixtures without detergent or urea. *J Proteome Res* 5, 3446-3452.
39. Haemmerle, G., Lass, A., Zimmermann, R., Gorkiewicz, G., Meyer, C., Rozman, J., Heldmaier, G., Maier, R., Theussl, C., Eder, S., Kratky, D., Wagner, E. F., Klingenspor, M., Hoefler, G., and Zechner, R. (2006) Defective lipolysis and altered energy metabolism in mice lacking adipose triglyceride lipase. *Science* 312, 734-737.
40. Duncan, R. E., Wang, Y., Ahmadian, M., Lu, J., Sarkadi-Nagy, E., and Sul, H. S. (2010) Characterization of desnutrin functional domains: critical residues for triacylglycerol hydrolysis in cultured cells. *J Lipid Res* 51, 309-317.
41. Menendez, J. A., Vazquez-Martin, A., Ortega, F. J., and Fernandez-Real, J. M. (2009) Fatty acid synthase: association with insulin resistance, type 2 diabetes, and cancer. *Clin Chem* 55, 425-438.
42. Beale, E. G., Hammer, R. E., Antoine, B., and Forest, C. (2002) Glyceroneogenesis comes of age. *FASEB J* 16, 1695-1696.
43. Olswang, Y., Cohen, H., Papo, O., Cassuto, H., Croniger, C. M., Hakimi, P., Tilghman, S. M., Hanson, R. W., and Reshef, L. (2002) A mutation in the peroxisome proliferator-activated receptor gamma-binding site in the gene for the cytosolic form of phosphoenolpyruvate carboxykinase reduces adipose tissue size and fat content in mice. *Proc Natl Acad Sci U S A* 99, 625-630.
44. Adler-Wailes, D. C., Guiney, E. L., Wolins, N. E., and Yanovski, J. A. (2010) Long-term ritonavir exposure increases fatty acid and glycerol recycling in 3T3-L1 adipocytes as compensatory mechanisms for increased triacylglycerol hydrolysis. *Endocrinology* 151, 2097-2105.
45. Brown, N. F., Hill, J. K., Esser, V., Kirkland, J. L., Corkey, B. E., Foster, D. W., and McGarry, J. D. (1997) Mouse white adipocytes and 3T3-L1 cells display an anomalous pattern of carnitine palmitoyltransferase (CPT) I isoform expression during differentiation.

Inter-tissue and inter-species expression of CPT I and CPT II enzymes. *Biochem J* 327 (Pt 1), 225-231.
46. De Pauw, A., Tejerina, S., Raes, M., Keijer, J., and Arnould, T. (2009) Mitochondrial (dys)function in adipocyte (de)differentiation and systemic metabolic alterations. *Am J Pathol* 175, 927-939.
47. Mallon, P. W., Unemori, P., Sedwell, R., Morey, A., Rafferty, M., Williams, K., Chisholm, D., Samaras, K., Emery, S., Kelleher, A., Cooper, D. A., and Carr, A. (2005) In vivo, nucleoside reverse-transcriptase inhibitors alter expression of both mitochondrial and lipid metabolism genes in the absence of depletion of mitochondrial DNA. *J Infect Dis* 191, 1686-1696.
48. Boothby, M., McGee, K. C., Tomlinson, J. W., Gathercole, L. L., McTernan, P. G., Shojaee-Moradie, F., Umpleby, A. M., Nightingale, P., and Shahmanesh, M. (2009) Adipocyte differentiation, mitochondrial gene expression and fat distribution: differences between zidovudine and tenofovir after 6 months. *Antivir Ther* 14, 1089-1100.
49. Sievers, M., Walker, U. A., Sevastianova, K., Setzer, B., Wagsater, D., Eriksson, P., Yki-Jarvinen, H., and Sutinen, J. (2009) Gene expression and immunohistochemistry in adipose tissue of HIV type 1-infected patients with nucleoside analogue reverse-transcriptase inhibitor-associated lipoatrophy. *J Infect Dis* 200, 252-262.
50. Kim, M. J., Jardel, C., Barthelemy, C., Jan, V., Bastard, J. P., Fillaut-Chapin, S., Houry, S., Capeau, J., and Lombes, A. (2008) Mitochondrial DNA content, an inaccurate biomarker of mitochondrial alteration in human immunodeficiency virus-related lipodystrophy. *Antimicrob Agents Chemother* 52, 1670-1676.
51. Coffinier, C., Hudon, S. E., Farber, E. A., Chang, S. Y., Hrycyna, C. A., Young, S. G., and Fong, L. G. (2007) HIV protease inhibitors block the zinc metalloproteinase ZMPSTE24 and lead to an accumulation of prelamin A in cells. *Proc Natl Acad Sci U S A* 104, 13432-13437.
52. Caron, M., Auclair, M., Donadille, B., Bereziat, V., Guerci, B., Laville, M., Narbonne, H., Bodemer, C., Lascols, O., Capeau, J., and Vigouroux, C. (2007) Human lipodystrophies linked to mutations in A-type lamins and to HIV protease inhibitor therapy are both associated with prelamin A accumulation, oxidative stress and premature cellular senescence. *Cell Death Differ* 14, 1759-1767.
53. Cox, A. G., Peskin, A. V., Paton, L. N., Winterbourn, C. C., and Hampton, M. B. (2009) Redox potential and peroxide reactivity of human peroxiredoxin 3. *Biochemistry* 48, 6495-6501.
54. Kang, S. W., Chae, H. Z., Seo, M. S., Kim, K., Baines, I. C., and Rhee, S. G. (1998) Mammalian peroxiredoxin isoforms can reduce hydrogen peroxide generated in response to growth factors and tumor necrosis factor-alpha. *J Biol Chem* 273, 6297-6302.
55. Findeisen, H. M., Pearson, K. J., Gizard, F., Zhao, Y., Qing, H., Jones, K. L., Cohn, D., Heywood, E. B., De Cabo, R., and Bruemmer, D. (2011) Oxidative Stress Accumulates in Adipose Tissue during Aging and Inhibits Adipogenesis. *PLoS One* 6, e18532.
56. Tang, H. L., Lung, H. L., Wu, K. C., Le, A. H., Tang, H. M., and Fung, M. C. (2008) Vimentin supports mitochondrial morphology and organization. *Biochem J* 410, 141-146.
57. Lieber, J. G., and Evans, R. M. (1996) Disruption of the vimentin intermediate filament system during adipose conversion of 3T3-L1 cells inhibits lipid droplet accumulation. *J Cell Sci* 109 (Pt 13), 3047-3058.

58. Franke, W. W., Hergt, M., and Grund, C. (1987) Rearrangement of the vimentin cytoskeleton during adipose conversion: formation of an intermediate filament cage around lipid globules. *Cell* 49, 131-141.
59. Kumar, N., Robidoux, J., Daniel, K. W., Guzman, G., Floering, L. M., and Collins, S. (2007) Requirement of vimentin filament assembly for beta3-adrenergic receptor activation of ERK MAP kinase and lipolysis. *J Biol Chem* 282, 9244-9250.
60. Prasad, R., Liu, Y., Deterding, L. J., Poltoratsky, V. P., Kedar, P. S., Horton, J. K., Kanno, S., Asagoshi, K., Hou, E. W., Khodyreva, S. N., Lavrik, O. I., Tomer, K. B., Yasui, A., and Wilson, S. H. (2007) HMGB1 is a cofactor in mammalian base excision repair. *Mol Cell* 27, 829-841.
61. Kang, R., Livesey, K. M., Zeh, H. J., Loze, M. T., and Tang, D. (2010) HMGB1: A novel Beclin 1-binding protein active in autophagy. *Autophagy* 6, 1209-1211.
62. Marino, G., Fernandez, A. F., and Lopez-Otin, C. (2010) Autophagy and aging: lessons from progeria models. *Adv Exp Med Biol* 694, 61-68.
63. Lamounier-Zepter, V., Bornstein, S. R., Kunes, J., Zicha, J., Krsek, M., Ehrhart-Bornstein, M., Ziegler, C. G., Kiessling, A., Funk, R. H., and Haluzik, M. (2008) Adrenocortical changes and arterial hypertension in lipoatrophic A-ZIP/F-1 mice. *Mol Cell Endocrinol* 280, 39-46.
64. Vettor, R., and Pagano, C. (2009) The role of the endocannabinoid system in lipogenesis and fatty acid metabolism. *Best Pract Res Clin Endocrinol Metab* 23, 51-63.
65. Huang, L. S., Hung, N. D., Sok, D. E., and Kim, M. R. (2010) Lysophosphatidylcholine containing docosahexaenoic acid at the sn-1 position is anti-inflammatory. *Lipids* 45, 225-236.
66. Cunningham, T. J., Yao, L., and Lucena, A. (2008) Product inhibition of secreted phospholipase A2 may explain lysophosphatidylcholines' unexpected therapeutic properties. *J Inflamm (Lond)* 5, 17.
67. Matsumoto, T., Kobayashi, T., and Kamata, K. (2007) Role of lysophosphatidylcholine (LPC) in atherosclerosis. *Curr Med Chem* 14, 3209-3220.
68. Damian D, Oresic M, Verheij E, Meulman JJ, and J, F. (2007) Applications of a new subspace clustering algorithm (COSA) in medical systems biology. *Metabolomics* 3, 69-77.
69. Pietilainen, K. H., Sysi-Aho, M., Rissanen, A., Seppanen-Laakso, T., Yki-Jarvinen, H., Kaprio, J., and Oresic, M. (2007) Acquired obesity is associated with changes in the serum lipidomic profile independent of genetic effects--a monozygotic twin study. *PLoS One* 2, e218.

FOOTNOTES

Mass spectrometry was performed at the Proteomics Facility (SCAI) of the University of Córdoba, which is Node 6 of the ProteoRed Consortium financed by Genoma España and belongs to the Andalusian Platform for Genomics, Proteomics and Bioinformatics. We thank Dr. M.S. Fernández-García for help with histopathological analysis. This work was supported by Ministerio de Ciencia e Innovación (MICINN)/FEDER (BFU2007-60180; BFU2010-

17116), Junta de Andalucía/FEDER (CTS-03039, and BIO-0139), and CIBER Obesidad y Nutrición (CIBERobn), Instituto de Salud Carlos III, Spain. C.L-O. laboratory is supported by grants from MICINN, Fundación M. Botín, and the European Union (FP7-Microenvimet). The Instituto Universitario de Oncología is supported by Obra Social Cajastur-Asturias, Spain. Metabolomics was performed by the Unit mix CIC bioGUNE- OWL Genomics.

FIGURE LEGENDS

Figure 1. Maturation of the lamin A precursor (prelamin A) requires several posttranslational processing steps: farnesylation of the C-terminal CaaX motif, proteolysis of the C-terminal aaX residues by endoproteases Zmpste24 and/or Rce1, carboxymethylation of the farnesylated cysteine and endoproteolysis of the 15 C-terminal amino acids by Zmpste24.

Figure 2. Lipoatrophy of visceral adipose tissue in *Zmpste24*$^{-/-}$ mice. A) Representative images showing adipose tissue distribution in 4-month-old *Zmpste24*$^{+/+}$ and *Zmpste24*$^{-/-}$ male mice. Loss of adipose tissue is evident in *Zmpste24*$^{-/-}$ mice (adipose tissue is indicated by a red line). B) Visceral adipose tissue removed from *Zmpste24*$^{+/+}$ and *Zmpste24*$^{-/-}$ animals. C) Comparisons of haematoxylin and eosin-stained cross sections of adipose tissue of *Zmpste24*$^{+/+}$ and *Zmpste24*$^{-/-}$ mice, showing the decreased size of adipocytes in *Zmpste24*-deficient mice. T, testis; AT, adipose tissue.

Figure 3. A) 2D-PAGE of whole adipose tissue of *Zmpste24*$^{+/+}$ and *Zmpste24*$^{-/-}$ mice. Proteins were separated on a 2-DE gel using 18 cm pH 3-10 NL strips in the first dimension and 12% SDS-PAGE gels in the second dimension. Molecular weights are indicated (right). Differentially expressed proteins between the adipose tissue samples are indicated with white

or black arrows. The numbers correspond to the spot numbers in Table 1. B) Magnification of the boxed region that contains protein pyruvate dehydrogenase β (quantified in middle graph) in 2D-PAGE gels corresponding to four *Zmpste24*$^{+/+}$ and four *Zmpste24*$^{-/-}$ mice. * $P < 0.05$.

Figure 4. Prelamin A accumulation in *Zmpste24*$^{-/-}$ mice. A) Accumulation of partially processed lamin A in *Zmpste24*-null mice could be observed in both bi-dimensional gels (pH: 3-10) and immunoblots (lower panel). B and C) Analysis of accumulated prelamin A by MALDI-TOF revealed that it corresponded to the methylated form of this protein (B), which does not carry the C-terminal aaX amino acids, as observed by MALDI–TOF analysis of the C-terminal tryptic peptides corresponding to the identified forms of prelamin A (1 and 2; C). A totally unprocessed form of prelamin A was not detected. Farn, Farnesylated; CM, Carboxymethylated.

Figure 5. Protein abundance (by Western blot) of malic enzyme (ME1; A), peroxiredoxin 3 (PRDX3; B), high-mobility group box-1 protein (HMGB1; C) and phosphoenolpyruvate carboxykinase 1 (PCK1; D) in adipose tissue from *Zmpste24*$^{+/+}$ (n=6) and *Zmpste24*$^{-/-}$ (n=4) mice. * $P < 0.05$, (±S.E.M.).

Figure 6. A) Magnification of a representative 2D-PAGE gel from *Zmpste24*$^{+/+}$ and *Zmpste24*$^{-/-}$ animals showing the area of the gel containing the 4 identified isoforms of vimentin (53, 49, 46 and 43 kDa approximately, left panel). All the isoforms were identified by western blot using the vimentin antibody (right panel). Two of the identified isoforms showed significant expression differences between the two groups of animals when evaluated

by western blot (B). C) Predicted molecular weight and isoelectric point of the identified forms of vimentin on the basis of MALDI-TOF identification.

Figure 7. Western blot for carnitine palmitoyltransferase I (CPT1; A) and uncoupling protein 1 (UCP1; B) in adipose tissue extracts. C) Analysis of ROS levels measured as relative fluorescence units (RFU) of DCF-DA, per ug of protein and minute. *Zmpste24*$^{+/+}$ (n=6) and *Zmpste24*$^{-/-}$ (n=4) mice * $P < 0.05$, (± S.E.M.).

Figure 8. A) Phosphoproteomic analysis of adipose tissue from *Zmpste24*$^{+/+}$ and *Zmpste24*$^{-/-}$ mice. B) The phospho-peptides identified by MALDI-TOF are indicated in the table. Potential phosphorylation sites are underlined. C: Carbamidomethyl. M_OX: Methionine Oxidated

Figure 9. Metabolic pathway analysis of the serum metabolomics experiments allowed for the identification of one statistically significant interaction map corresponding to free radical scavenging, lipid metabolism and small molecule biochemistry (top). 9 of the identified metabolites were identified to belong to this pathway (bottom).

Figure 10. Schematic representation of the metabolic pathways altered in adipose tissue of *Zmpste24*$^{-/-}$ mice. Up-regulated (blue) and down-regulated (green) proteins are highlighted. Proteins with more than a 3-fold increase between wild type and null mice are indicated with a double arrow.

Table 1 A. Proteins identified by MALDI-TOF/TOF up-regulated in ZMPSTE24-/-

Spot Num.[a]	Protein name	Symbol	Accesion number[b]	MW (kDa)/pI	% Cover.[c]	Pep.[d]	Protein E-value[e]	Mean fold change[f]	*P Student´s t-test*[g]
1	Fatty acid synthase	FAS	CH466558	276.7/6.2	12	25	44	3,61	0.002
2	Pyruvate carboxylase	PC	EDL33053	130.3/6.2	48	46	118	2,51	0.001
3	ATP citrate lyase [h]	ACLY	NP_598798	120.5/7.3	40	43	102	2,80	0002
4	Mitochondrial inner membrane protein	IMMT	NP_083949	84.2/6.2	36	30	33	1,96	0.037
5	Aconitase 2, mitochondrial	ACO2	NP_542364	86.3/8.1	50	37	116	2,38	0.003
6	Lamin A, precursor	PRELA-MIN	NP_733821	74.5/6.5	46	30	66	> 10	
7	Acyl-CoA synthetase long-chain family member 1	ACSL1	NP_032007	78.9/6.8	42	27	83	1,88	0.044
8	Propionyl CoA-carboxylase alpha-subunit	PCCA	AAL02364	80.2/7.0	56	37	100	1,98	0.013
9	Glycerol-3-phosphate dehydrogenase, mit. precursor (GPD-M)	GPD2	Q64521	81.4/6.2	55	41	92	2,54	0.001
10	Succinate dehydrogenase	SDHA	NP_075770	73.62/7.1	48	14	15	1,62	0.048
11	Transketolase	TKT	NP_033414	68.3/7.2	63	34	139	1,77	0.010
12	Malic enzyme 1, NADP (+)-dependent, cytosolic	ME1	NP_032641	64.5/7.2	62	33	159	2,34	0.022
13	Glucose-6-phosphate 1-dehydrogenase	G6PD	NP_032088	59.7/ 6.1	55	40	112	1,64	0.008
14	Mitochondrial aldehyde dehydrogenase 2	ALDH2	EDL19719	55.2/8.3	54	28	159	1,71	0.005
15	Desnutrin [h]	ATGL	AAU33824	54.4/6.0	34	22	37	1,79	0.036
16	mCG3880 [similar to Al-dehyde dehydrogenase family 3 member B1]		EDL32976	52.7/6.2	32	19	36	1,44	0.050

17	Pyruvate dehydrogenase protein X	PDHX	NP_780303	54.2/7.6	35	19	31	1,79	0.020
18	Atp5b protein	ATP5B	AAH37127	56.7/5.2	64	25	112	1,40	0.018
19	Ubiquinol-cytochrome c reductase core protein 1	UQCRC1	NP_079683	53.3/5.7	48	21	86	1,84	0.039
20	2-Oxoglutarate dehydrogenase complex component E2	DLST	Q01205	49.2/8.9	38	19	37	3,55	0.002
21	Enolase 1, alpha non-neuron	ENO1	AAH03891	47.5/6.2	80	24	116	1,35	0.003
22	Succinyl-CoA ligase [GDP-forming] subunit beta	SUCLG2	NP_035637	47.1/6.6	39	16	60	1,78	0.035
23	Acyl-Coenzyme A dehydrogenase, Short/branched chain	ACADS	AAH54428	48.3/8.0	33	19	56	2,25	0.001
24	NADH dehydrogenase (ubiquinone) 1 alpha subcomplex 10[h]	NDUFA10	NP_077159	40.1/6.4	37	23	62	2,19	0.025
25	Acyl-CoA thioesterase 2, mitochondrial precursor	ACOT2	Q9QYR9	49.8/6.9	52	19	48	2,15	0.006
26	Citrate synthase, mitochondrial precursor	CS	NP_080720	51.9/8.7	31	18	42	2,23	0.009
27	Glutamate-ammonia ligase	GLUL	AAA17989	42.8 /6.6	54	23	39	1,64	0.010
28	Isocitrate dehydrogena-se 3 (NAD+) alpha,	IDH3B	EDL25822	35.0/5.9	62	25	96	1,68	0.001
29	3-hydroxyisobutyryl-Coenzyme A hydrolase	HIBCH	EDK99981	43.34/8.2	59	24	60	1,63	0.050
30	Transaldolase 1	TALDO1	EDL18063	31.7/7.7	62	19	61	3,27	0.004
31	Pyruvate dehydrogenase (lipoamide) beta	PDHB	NP_077183	39.2/6.4	63	18	69	2,56	0.005
32	Branched-chain-amino-acid aminotransferase,mit.	BCATm	NP_033867	44.7/8.6	40	16	59	3,20	0.035
33	Glycerol-3-phosphate dehydrogenase	GPD1	AAA37726	38.2/6.7	68	26	68	1,74	0.009
34	Malate dehydrogenase, cytoplasmic	MDH1	NP_032644	36.6/6.2	38	13	89	1,41	0.011
35	3-hydroxyisobutyrate dehydrogenase	HIBADH	BAF42049	35.89/8.9	45	17	63	1,68	0.028

36	High mobility group box 1	HMGB1	NP_034569	24.8/6.4	57	16	47	1,87	0.023
37	Peroxiredoxin 3	PRDX3	NP_031478	28.3/7.1	31	11	104	1,45	0.009

Table 1B. Proteins identified by MALDI-TOF/TOF down-regulated in ZMPSTE24-/-

Spot Num. [a]	**Protein name**	**Symbol**	**Accesion number**[b]	**MW (kDa)/pI**	**% Cover.** [c]	**Pep.** [d]	**Protein E-value** [e]	**Mean fold change**[f]	***P Student´s t-test*** [g]
1	Gelsolin precursor	GELSOLIN	NP_666232	86.3/5.83	35	20	31	1,69	0.007
2	Phosphoenolpyruvate carboxykinase 1, cytosolic	PECK	AAH37629	70.1/6.18	33	23	71	1,54	0.042
3	Vimentin	VIM	NP_035831	51.6/5.0	61	34	100	1,41	0.004
4	Alpha-1-antitrypsin	SERPIN 1A	AAH10988	47.3/5.2	41	17	47	1,55	0.014
5	Phosphoglycerate dehydrogenase	PHGDH	NP_058662	57.3/6.3	26	26	81	1,70	0.001
6	Vimentin	VIM	NP_035831	53.7/5.1 Observed (≈49)	66	33	107	1,88	0.067
7	Vimentin	VIM	NP_035831	53.7/5.1 Observed (≈46)	65	32	85	3,34	0.01
8	Vimentin	VIM	NP_035831	53.7/5.1 Observed (≈43)	64	36	103	5,55	0.009
9	Alpha-2-macroglobulin 35 kDa subunit, precursor	A2M	Q61838	167.1/ 6.2	43	15	33	1,70	0.01

[a] Spot numbers correspond to those on Fig. 3A, right panel.
[b] Accession number from the NCBInr database.
[c] Coverage of all peptide sequences matched to the identified protein sequence (%).
[d] Pep. corresponds to the number of peptides identified (Mascot).
[e] X!Tandem E-value after reverse database search [Data represented as –Log(E-value].
[f] Mean fold change indicates the average volume ratio of 4 *Zmpste24*$^{+/+}$ and 4 *Zmpste24*$^{-/-}$ animals.
[g] Only those proteins with a $P < 0.05$ (Student's t-test) were considered.
[h] Phosphorylated proteins also detected by ProQ-Diamond Staining.

Fig. 1.

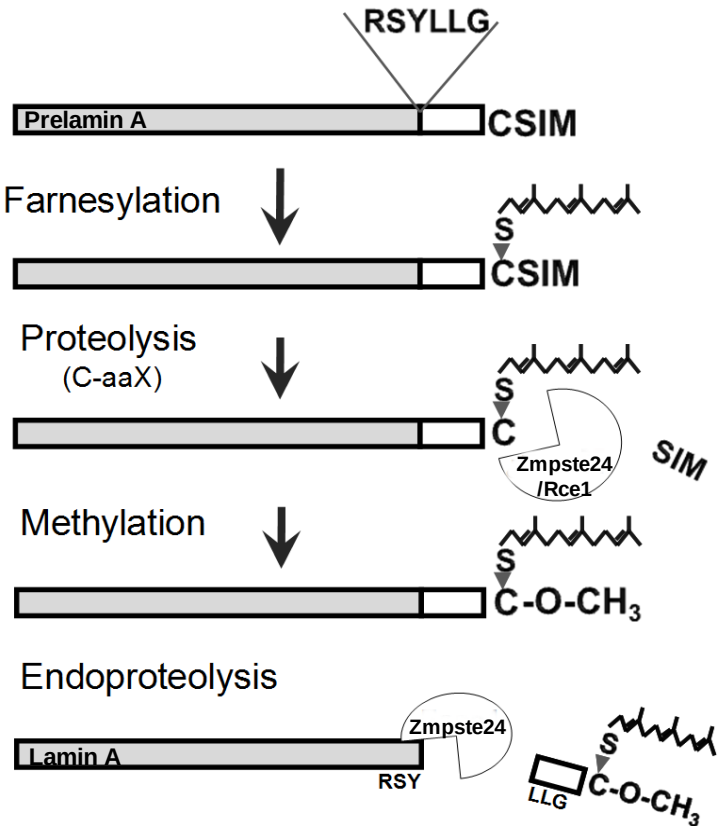
RSYLLG
Prelamin A
CSIM
Farnesylation
S
CSIM
Proteolysis
(C-aaX)
S
C
Zmpste24
/Rce1
SIM
Methylation
S
C-O-CH3
Endoproteolysis
Zmpste24
Lamin A
RSY
S
LLG
C-O-CH3

Fig. 2.

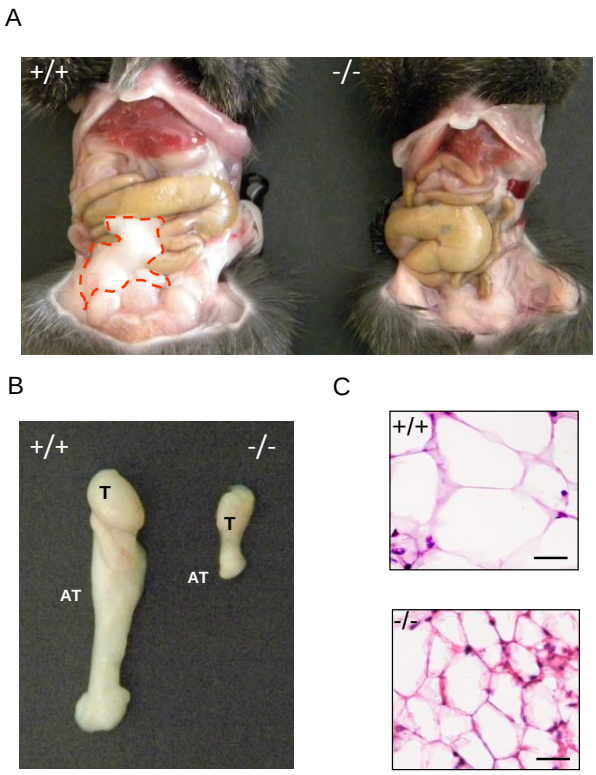

Fig. 3.

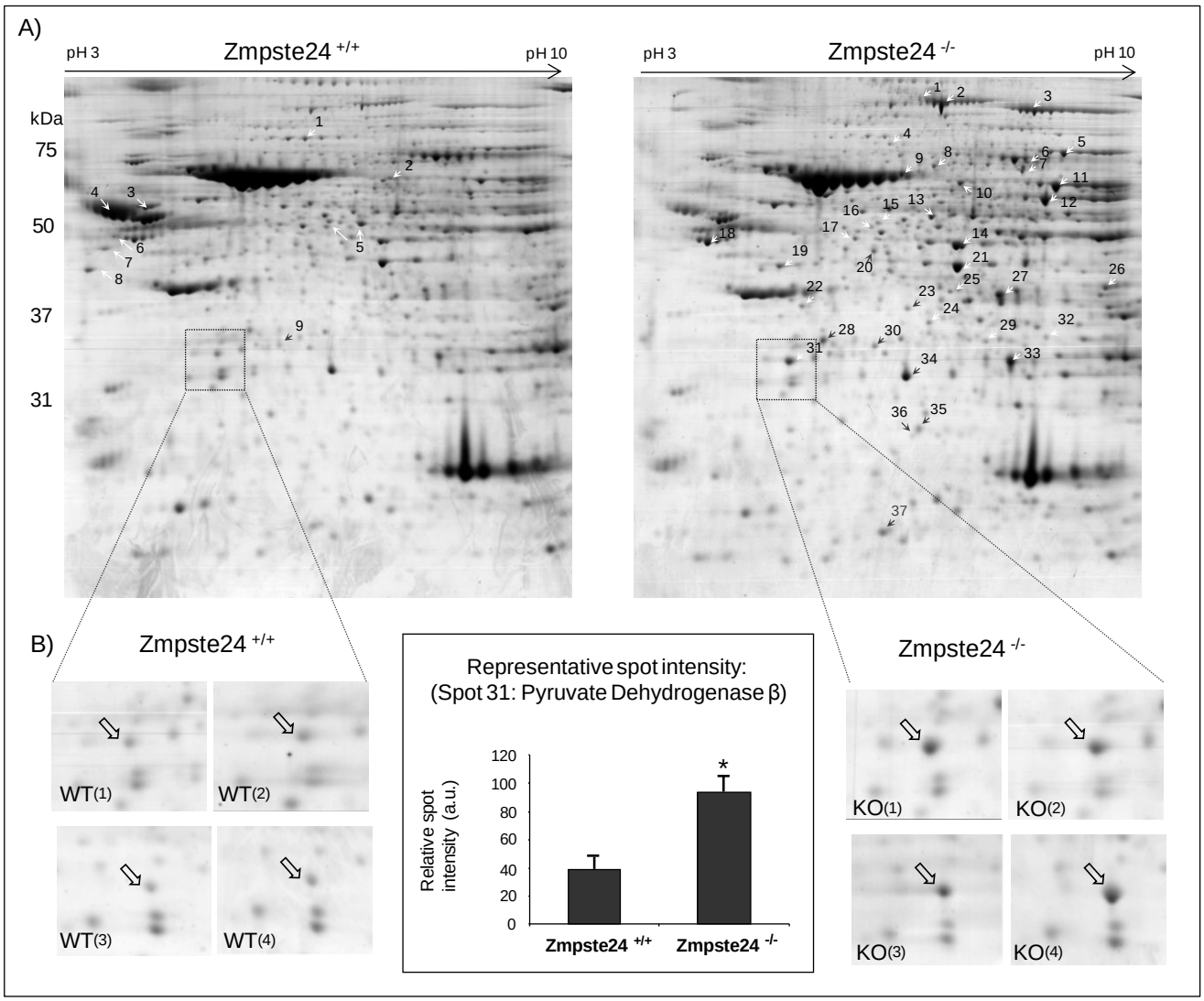
A)
pH 3
Zmpste24 +/+
pH 10
kDa
75
50
37
31
pH 3
Zmpste24 -/-
pH 10
B)
Zmpste24 +/+
WT(1)
WT(2)
WT(3)
WT(4)
Representative spot intensity:
(Spot 31: Pyruvate Dehydrogenase β)
Relative spot intensity (a.u.)
120
100
80
60
40
20
0
*
Zmpste24 +/+
Zmpste24 -/-
Zmpste24 -/-
KO(1)
KO(2)
KO(3)
KO(4)

Fig. 4.

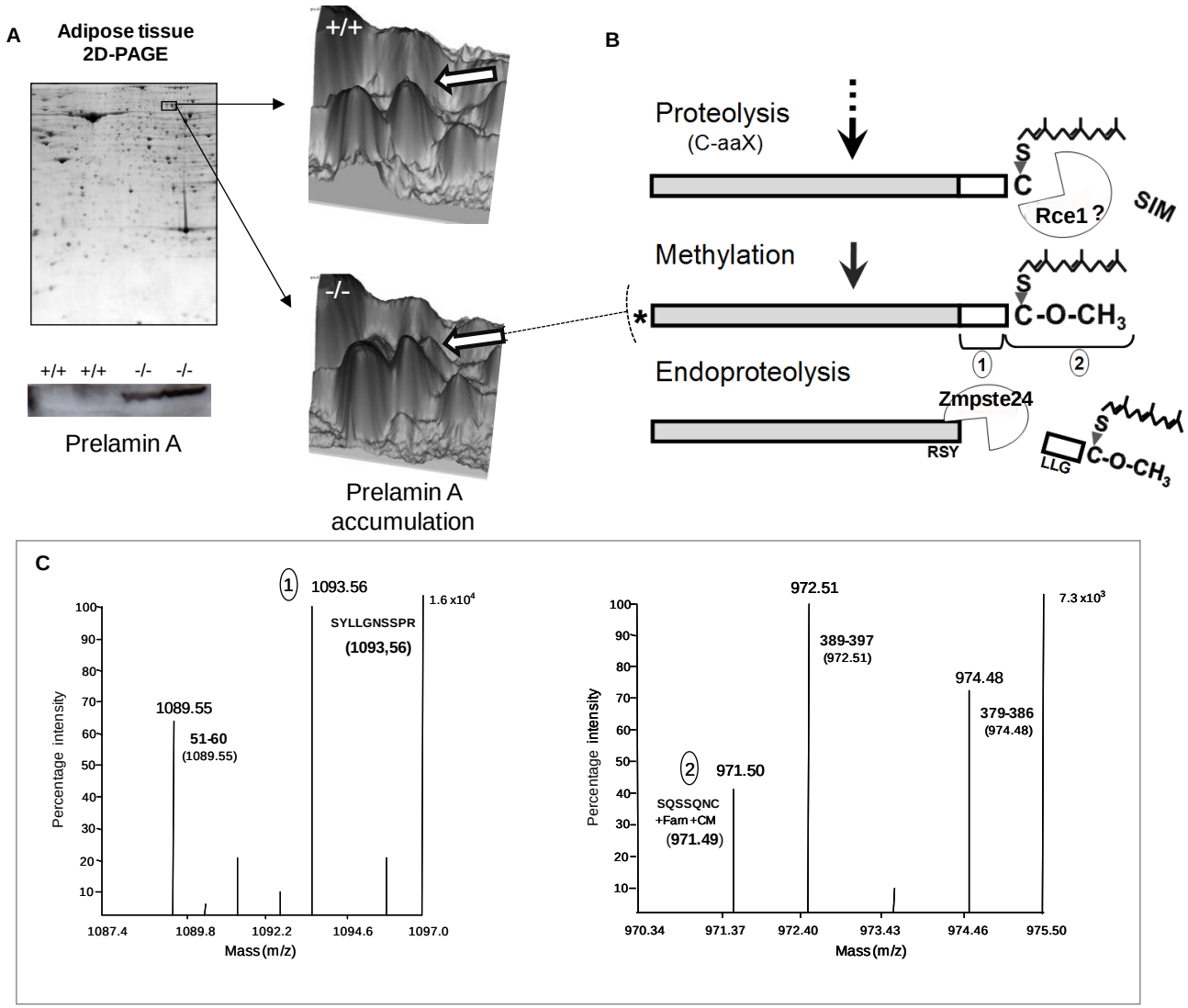
A
Adipose tissue
2D-PAGE
+/+
-/-
+/+ +/+ -/- -/-
Prelamin A
Prelamin A
accumulation
B
Proteolysis
(C-aaX)
Rce1 ?
SIM
Methylation
Endoproteolysis
Zmpste24
RSY
LLG
C
1093.56
SYLLGNSSPR
(1093,56)
1089.55
51-60
(1089.55)
Percentage intensity
Mass (m/z)
972.51
389-397
(972.51)
974.48
379-386
(974.48)
971.50
SQSSQNC
+Fam+CM
(971.49)

Fig. 5.

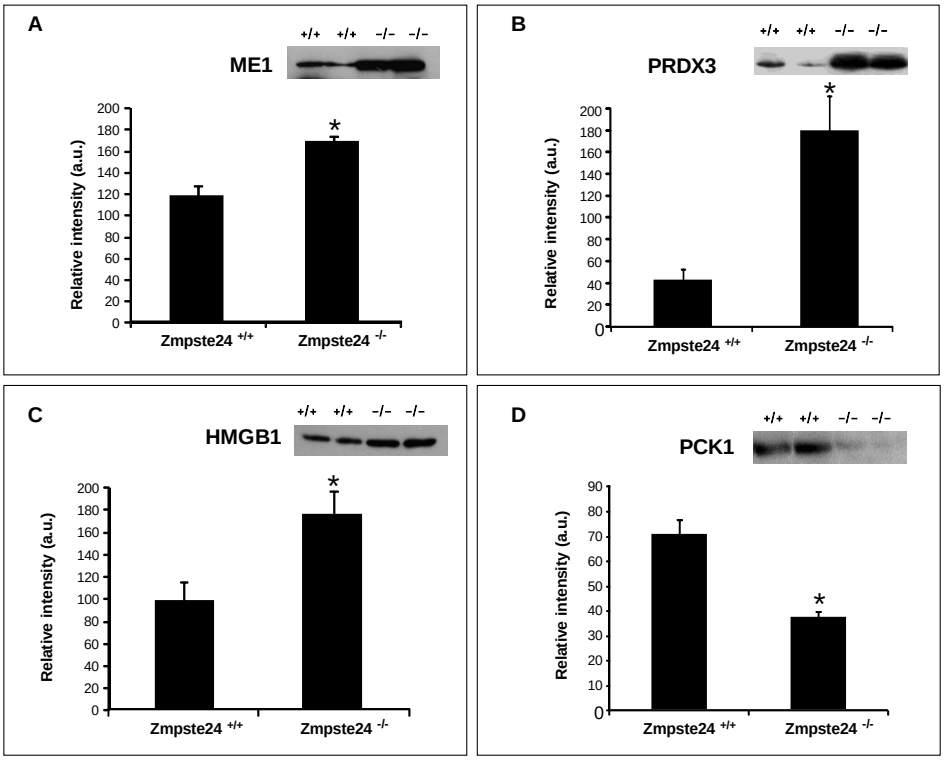
A
+/+ +/+ −/− −/−
ME1
Relative intensity (a.u.)
200
180
160
140
120
100
80
60
40
20
0
*
Zmpste24 +/+
Zmpste24 -/-
B
+/+ +/+ −/− −/−
PRDX3
Relative intensity (a.u.)
200
180
160
140
120
100
80
60
40
20
0
*
Zmpste24 +/+
Zmpste24 -/-
C
+/+ +/+ −/− −/−
HMGB1
Relative intensity (a.u.)
200
180
160
140
120
100
80
60
40
20
0
*
Zmpste24 +/+
Zmpste24 -/-
D
+/+ +/+ −/− −/−
PCK1
Relative intensity (a.u.)
90
80
70
60
50
40
30
20
10
0
*
Zmpste24 +/+
Zmpste24 -/-

Fig. 6.

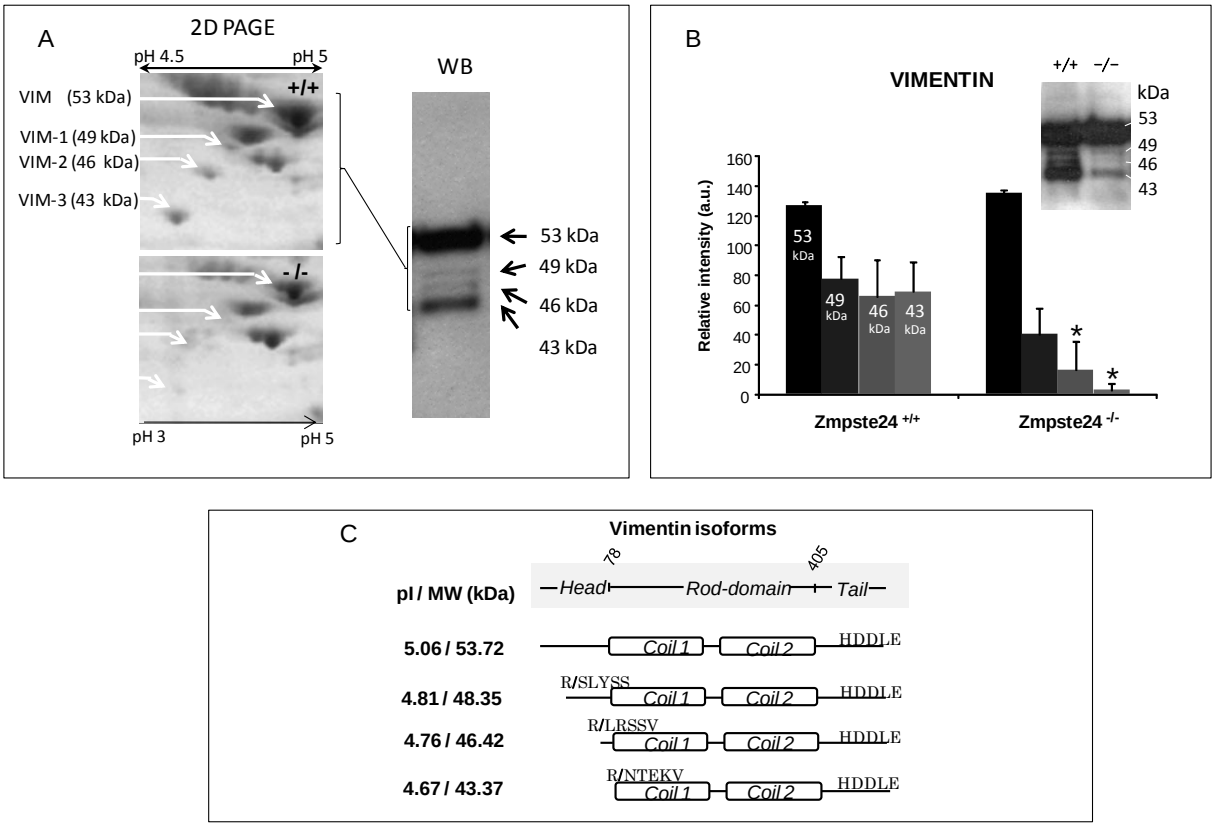
A
2D PAGE
pH 4.5
pH 5
VIM (53 kDa)
VIM-1 (49 kDa)
VIM-2 (46 kDa)
VIM-3 (43 kDa)
+/+
- /-
pH 3
pH 5
WB
53 kDa
49 kDa
46 kDa
43 kDa
B
VIMENTIN
+/+ −/−
kDa
53
49
46
43
Relative intensity (a.u.)
160
140
120
100
80
60
40
20
0
53 kDa
49 kDa
46 kDa
43 kDa
*
*
Zmpste24 +/+
Zmpste24 -/-
C
Vimentin isoforms
pI / MW (kDa)
78
405
Head
Rod-domain
Tail
5.06 / 53.72
Coil 1
Coil 2
HDDLE
4.81 / 48.35
R/SLYSS
4.76 / 46.42
R/LRSSV
4.67 / 43.37
R/NTEKV

Fig. 7.

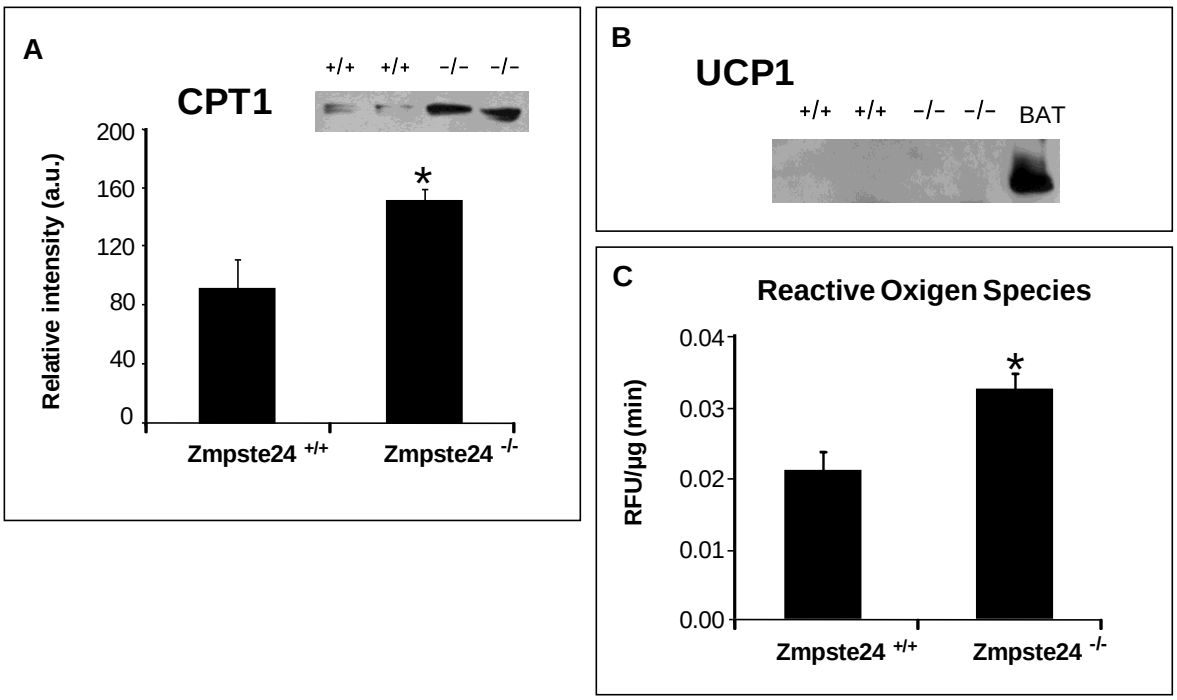
A
CPT1
+/+ +/+ −/− −/−
Relative intensity (a.u.)
200
160
120
80
40
0
*
Zmpste24 +/+
Zmpste24 -/-
B
UCP1
+/+ +/+ −/− −/− BAT
C
Reactive Oxigen Species
RFU/µg (min)
0.04
0.03
0.02
0.01
0.00
*
Zmpste24 +/+
Zmpste24 -/-

Fig. 8

A

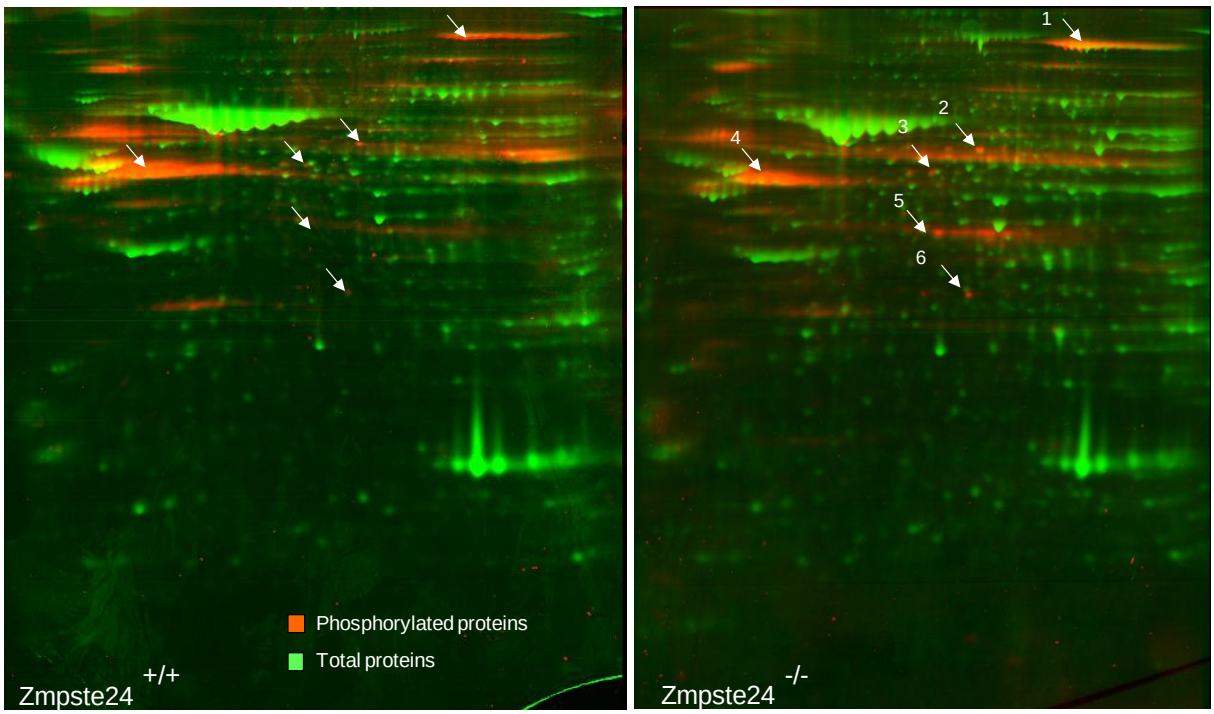

B

Name	Phospho.Detected Peptide	Score deviation (Da)
1) ACLY-1	Not Determined	
2) PGM-1	108-130 AIGGIIL**T**ASHNPGGPNGDFGIK,	0.0207.
	86-105 LVIGQNGIL**ST**PAVSCIIRK,	0.0068 (C)[8].
3) Desnutrin	444-462 QLLLGLFC**T**NVAFPPDALR,	-0.001 (C)[8].
4) Desmin	38 52 AGFG**T**KGSSSSMTSR	0.059 (M_OX)[12]
5) PDHA1	Not Determined	
6) NDUFA10	Not Determined	

Fig. 9.

Top Networks

ID	Associated Network Functions	Score
1	Free Radical Scavenging, Lipid Metabolism, Small Molecule Biochemistry	25
2	Cardiovascular System Development and Function, Cell Morphology, Embryonic Development	1
3	Small Molecule Biochemistry, Gene Expression, Lipid Metabolism	0

INGENUITY SYSTEMS

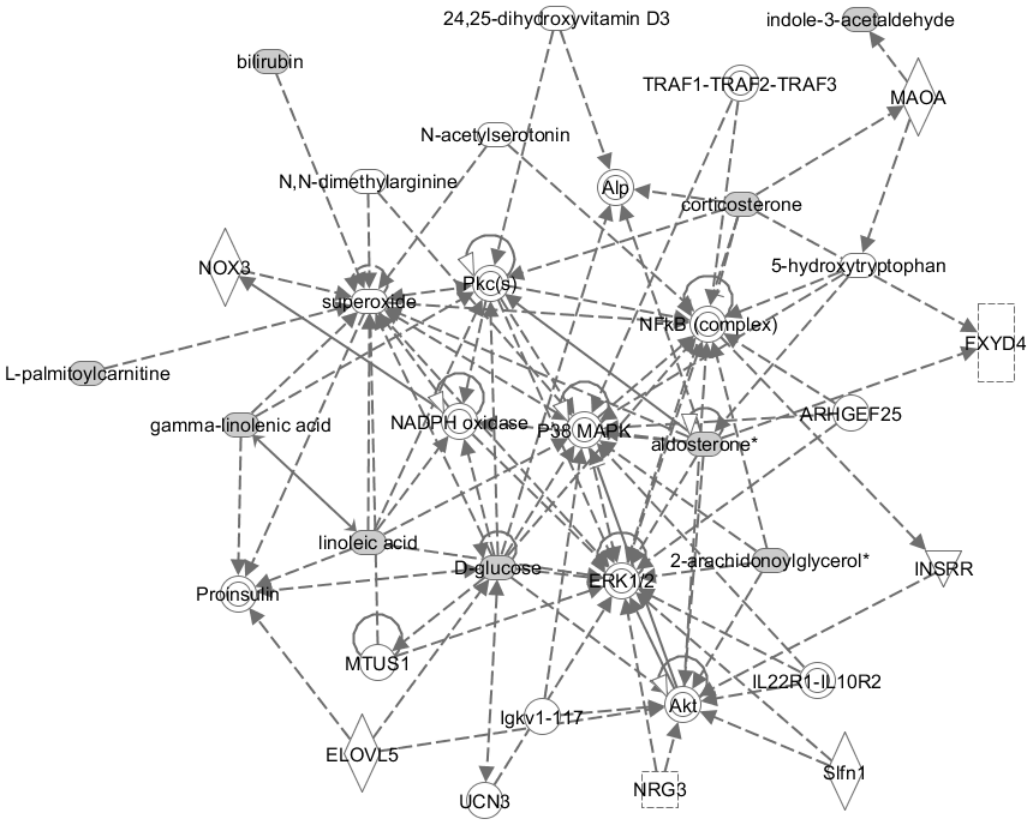

1 Free Radical Scavenging, Lipid Metabolism, Small Molecule Biochemistry

Fig.10.

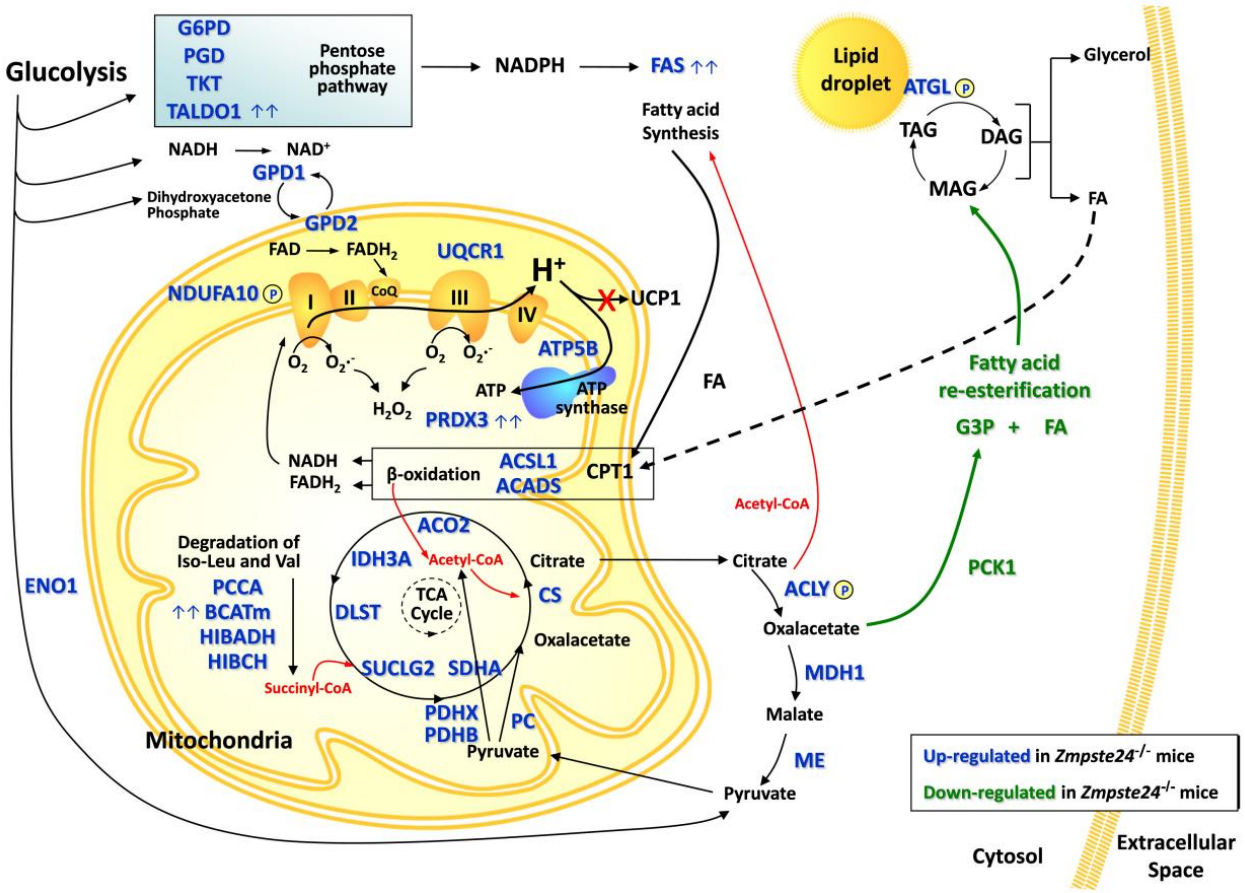
Glucolysis
G6PD
PGD
TKT
TALDO1 ↑↑
Pentose phosphate pathway
NADPH
FAS ↑↑
Fatty acid Synthesis
Lipid droplet
ATGL
Glycerol
TAG
DAG
MAG
FA
NADH
NAD+
GPD1
Dihydroxyacetone Phosphate
GPD2
FAD
FADH2
UQCR1
H+
NDUFA10
I
II
CoQ
III
IV
UCP1
O2
O2·-
ATP5B
ATP
ATP synthase
H2O2
PRDX3 ↑↑
FA
Fatty acid re-esterification
G3P + FA
NADH
FADH2
β-oxidation
ACSL1
ACADS
CPT1
Acetyl-CoA
ACO2
IDH3A
Acetyl-CoA
Citrate
Citrate
Degradation of Iso-Leu and Val
PCCA
↑↑ BCATm
HIBADH
HIBCH
DLST
TCA Cycle
CS
ACLY
PCK1
ENO1
Oxalacetate
Oxalacetate
MDH1
Malate
Succinyl-CoA
SUCLG2
SDHA
PDHX
PDHB
PC
Pyruvate
ME
Pyruvate
Mitochondria
Up-regulated in Zmpste24-/- mice
Down-regulated in Zmpste24-/- mice
Cytosol
Extracellular Space